Identification of a Stelar-Localized Transport Protein That Facilitates Root-to-Shoot Transfer of Chloride in Arabidopsis[1][OPEN]

Bo Li, Caitlin Byrt, Jiaen Qiu, Ute Baumann, Maria Hrmova, Aurelie Evrard, Alexander A.T. Johnson, Kenneth D. Birnbaum, Gwenda M. Mayo, Deepa Jha, Sam W. Henderson, Mark Tester*, Mathew Gilliham*, and Stuart J. Roy

Australian Centre for Plant Functional Genomics (B.L., J.Q., U.B., M.H., A.E., D.J., M.T., S.J.R.), School of Agriculture, Food, and Wine (B.L., C.B., J.Q., U.B., M.H., A.E., G.M.M., D.J., S.W.H., M.T., M.G., S.J.R.), and ARC Centre of Excellence in Plant Energy Biology (C.B., J.Q., S.W.H., M.G.), University of Adelaide, SA 5064, Australia; Centre for Desert Agriculture, King Abdullah University of Science and Technology, Thuwal 23955-6900, Kingdom of Saudi Arabia (B.L., M.T.); School of BioSciences, University of Melbourne, Parkville, Vic 3010, Australia (A.A.T.J.); and Centre for Genomics and Systems Biology, New York University, New York 10003 (K.D.B.)

ORCID IDs: 0000-0001-8549-2873 (C.B.); 0000-0001-9220-4219 (J.Q.); 0000-0003-3019-1891 (S.W.H.); 0000-0002-5085-8801 (M.T.); 0000-0003-0666-3078 (M.G.); 0000-0003-0411-9431 (S.J.R.).

Under saline conditions, higher plants restrict the accumulation of chloride ions (Cl^-) in the shoot by regulating their transfer from the root symplast into the xylem-associated apoplast. To identify molecular mechanisms underpinning this phenomenon, we undertook a transcriptional screen of salt stressed Arabidopsis (*Arabidopsis thaliana*) roots. Microarrays, quantitative RT-PCR, and promoter-GUS fusions identified a candidate gene involved in Cl^- xylem loading from the Nitrate transporter 1/Peptide Transporter family (*NPF2.4*). This gene was highly expressed in the root stele compared to the cortex, and its expression decreased after exposure to NaCl or abscisic acid. NPF2.4 fused to fluorescent proteins, expressed either transiently or stably, was targeted to the plasma membrane. Electrophysiological analysis of NPF2.4 in *Xenopus laevis* oocytes suggested that NPF2.4 catalyzed passive Cl^- efflux out of cells and was much less permeable to NO_3^-. Shoot Cl^- accumulation was decreased following *NPF2.4* artificial microRNA knockdown, whereas it was increased by overexpression of *NPF2.4*. Taken together, these results suggest that NPF2.4 is involved in long-distance transport of Cl^- in plants, playing a role in the loading and the regulation of Cl^- loading into the xylem of Arabidopsis roots during salinity stress.

[1] This work was funded by the Australian Research Council (ARC), Grains Research and Development Corporation (GRDC), and the King Abdullah University for Science and Technology funding to M.T., GRDC funding (UA00145) to S.J.R. and M.G., and ARC Centre of Excellence (CE140100008) and ARC Future Fellowship (FT130100709) funding to M.G.

* Address correspondence to mark.tester@kaust.edu.sa or matthew.gilliham@adelaide.edu.au.

The author responsible for distribution of materials integral to the findings presented in this article in accordance with the policy described in the Instructions for Authors (www.plantphysiol.org) is: Mathew Gilliham (matthew.gilliham@adelaide.edu.au).

B.L. performed the majority of the experiments and analysis and drafted the manuscript; C.B. conducted experiments for Fig. 7, A and E to H; J.Q. conducted experiments for Fig. 7, H and I; K.D.B. advised and assisted with the fluorescent-activated cell sorting; A.E., A.A.T.J., and U.B. analyzed the microarray data; G.M.M. developed the assays for the cross sections of GUS plant roots; M.H. constructed 3D protein models; D.J. characterized putative *npf2.4* knockout lines; S.W.H. assisted with the $^{36}Cl^-$ flux assays; M.T. conceived the research and identified the candidate gene; M.G and S.J.R. supervised the research and cowrote the manuscript; all authors commented on the manuscript.

[OPEN] Articles can be viewed without a subscription.

www.plantphysiol.org/cgi/doi/10.1104/pp.15.01163

Soil salinity is a significant threat to world agriculture as it restricts plant growth and decreases the yield of crops (Munns, 2002; Munns and Tester, 2008; Roy et al., 2014). To feed a rapidly growing global population, world food production needs to increase by 70–110% before 2050 (Tilman et al., 2011). Compounding matters, the area of salt affected farmland is expanding as a consequence of less frequent rainfall, irrigation with suboptimal water, and rising water tables (Rengasamy, 2002, 2006). To meet the food demand of future generations, improving crop salinity tolerance is a high priority. One approach to enhance plant salinity tolerance is to minimize salt (NaCl) accumulation in the cytoplasm of the shoot, a primary site of salt damage, while maintaining the uptake of beneficial ions such as nitrate (NO_3^-) and potassium (K^+) (Munns, 2002; Tester and Davenport, 2003; Teakle and Tyerman, 2010).

Improving salt exclusion from the shoot is one means of enhancing plant salinity tolerance (Apse and Blumwald, 2007; Munns and Tester, 2008; Horie et al., 2009; Munns et al., 2012; Guan et al., 2014). Significant progress has been made in characterizing the genes encoding proteins that are central to regulating shoot

 © 2016 American Society of Plant Biologists. All Rights Reserved.

Na^+ accumulation during salt stress (Roy et al., 2014; Munns and Gilliham, 2015). In particular, the functions of the high affinity K^+ transporter *HKT* gene family (Uozumi et al., 2000; Mäser et al., 2002; Berthomieu et al., 2003; Davenport et al., 2007; Waters et al., 2013; Byrt et al., 2014) and the Na^+/H^+ antiporter and salt overly sensitive (*SOS*) gene families (Wu et al., 1996; Shi et al., 2000, 2002; Qiu et al., 2002; Bassil and Blumwald, 2014) have been areas of intensive research. Manipulation of these pathways has led to improvements in the salt tolerance of the model plant Arabidopsis (*Arabidopsis thaliana*; Sunarpi et al., 2005; Møller et al., 2009) and crops (Ren et al., 2005; James et al., 2006; Byrt et al., 2007; Plett et al., 2010; Qiu et al., 2011; Munns et al., 2012). Excessive chloride ion (Cl^-) accumulation in the cytoplasm of plant cells, particularly in the shoot, is also toxic to plants (Tyerman, 1992; Xu et al., 1999; Munns and Tester, 2008; Teakle and Tyerman, 2010; Geilfus et al., 2015), resulting in a reduction in plant growth and symptoms such as leaf burn and leaf abscission for Cl^--sensitive species (Abel, 1969; Parker et al., 1983; Cole, 1985). Cl^-, rather than sodium ions (Na^+), is considered to be the more toxic ion for woody perennial species such as grapevine (*Vitis vinifera*; Tregeagle et al., 2006; Gong et al., 2011) and citrus (*Citrus jambhiri*; Storey and Walker, 1999) and legumes such as soybean (*Glycine max*; Luo et al., 2005) and lotus (*Lotus tenuis*; Teakle et al., 2007). For cereal crops such as wheat (*Triticum aestivum*; Martin and Koebner, 1995) and barley (*Hordeum vulgare*; Tavakkoli et al., 2011), the toxic effects of Cl^- and Na^+ are additive and can often be overcome by restricting excess accumulation of both ions in the shoot. It has also been shown that the xylem-sap Cl^- content of salt-tolerant genotypes of wheat (Läuchli et al., 2008), citrus (Moya et al., 2003), and lotus (Teakle et al., 2007) is lower when compared with salt sensitive genotypes, suggesting that the control of Cl^- concentration in the transpiration stream is a contributing factor to plant salinity tolerance. However, the molecular determinants of long-distance Cl^- transport in plants and how it is regulated in response to salinity stress are still largely unknown (Teakle and Tyerman, 2010; Henderson et al., 2014). While some candidate proteins, such as cation-Cl^- cotransporters in Arabidopsis (Colmenero-Flores et al., 2007) and rice (*Oryza sativa*; Kong et al., 2011) have been proposed to retrieve Cl^- from the xylem, there are still unresolved questions in regard to their localization and mode of action (Teakle and Tyerman, 2010; Henderson et al., 2015).

Chloride is a micronutrient required by all plants, functioning as a key regulator of turgor (and stomatal movement), membrane potential, and cytosolic pH (Xu et al., 1999; White and Broadley, 2001; Teakle and Tyerman, 2010). Cl^- is acquired by plants from the soil at low concentrations by active symport with H^+ (Sanders, 1980; Beilby and Walker, 1981; Felle, 1994) and passively enters the plant at high concentrations due to a reversal in the electrochemical potential (Skerrett and Tyerman, 1994). Casparian bands in the endodermis limit the transfer of Cl^- through an apoplastic pathway; thus, most Cl^- ions move from cell to cell toward xylem vessels following the symplastic pathway (Pitman, 1982). This means Cl^- must cross root plasma membranes at least twice for it to be loaded into the xylem vessels, prior to being transferred to the shoot via the transpiration stream. Due to the measured ion concentrations in root cytoplasm and the xylem, the loading of Cl^- into the root xylem is highly likely to be electrochemically passive, and it is thus likely to be facilitated by plasma membrane localized anion channels or carriers that are not yet identified (White and Broadley, 2001; Munns and Tester, 2008; Teakle and Tyerman, 2010; Kollist et al., 2011; Henderson et al., 2014).

While little is known about the genes and proteins responsible for Cl^- loading into the root xylem apoplast, more is known about the biological processes involved. Abscisic acid (ABA) was shown to significantly inhibit xylem loading of Cl^-, as well as K^+ (Rb^+), while having a limited effect on the initial uptake of these ions from the external medium. This leads to an accumulation of both Cl^- and K^+ ions in the root and results in a reduced delivery to the shoot (Cram and Pitman, 1972; Pitman et al., 1974; Pitman, 1977). The discovery of the gene underlying K^+ xylem loading, the stelar outwardly rectifying K^+ channel (*SKOR*), illustrated that ABA down-regulates the K^+ flux to the xylem vessels at both a transcriptional and a posttranslational level (Gaymard et al., 1998; Roberts, 1998; Roberts and Snowman, 2000). Electrophysiological studies of maize (*Zea mays*) and barley root xylem parenchyma cells identified three conductances that could facilitate the passive xylem loading of anions such as Cl^- and NO_3^- into the xylem apoplast: xylem-parenchyma quickly activating anion conductance (X-QUAC), xylem-parenchyma

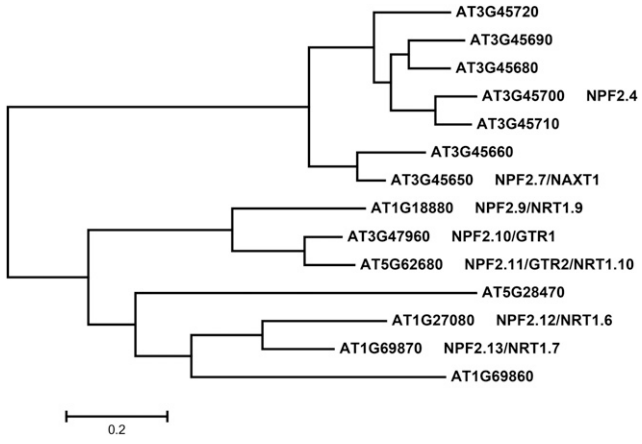

Figure 1. Bioinformatic analysis of NPF2.4. Phylogenetic tree shows relationships between the seven members of the NAXT subfamily (the uppermost 7 genes) and seven other NPF2s. Multiple amino acid sequence alignment was performed with ClustalW2 with a gap open of 10 and a gap extension of 0.1. Phylogenetic tree was generated using MEGA package 5.0 with default settings. Names are shown for proteins that are available in literature. Bar indicates the maximum likelihood distance.

slowly activating anion conductance, and xylem-parenchyma inwardly rectifying anion conductance (Köhler and Raschke, 2000; Köhler et al., 2002; Gilliham and Tester, 2005). X-QUAC, the anion conductance most likely to be responsible for the majority of Cl^- xylem loading, was significantly down-regulated when plants were treated with ABA (Gilliham and Tester, 2005).

Here, we identified a gene encoding an anion transport protein with properties that are consistent with a role in Cl^- loading into the root xylem apoplast in Arabidopsis. The knowledge gained here opens avenues for manipulation of these pathways in Cl^--sensitive species for improving salinity tolerance.

RESULTS

Identification of Candidate Genes Encoding Transporters for Cl^- Xylem Loading in Arabidopsis

Based on accumulated physiological evidence, it was hypothesized that the rate-limiting step of Cl^- loading to the shoot is in the root stele and is ultimately regulated by transcription of genes encoding Cl^- transporters (Gilliham and Tester, 2005; Teakle and Tyerman, 2010; Henderson et al., 2014). Previously, a comparative transcriptomic analysis of pericycle and cortical cells in the root of Arabidopsis in response to salt (50 mM NaCl for 2 d) had been conducted using fluorescent-activated cell sorting and Affymetrix microarrays (Evrard et al., 2012; Evrard, 2013). The data were subsequently reanalyzed to identify stelar-expressed genes that were likely to encode membrane bound anion permeable transport proteins that had their expression reduced by salt stress. Two candidates were identified that satisfied these criteria from this preliminary screen: the known H^+/NO_3^- symporter (*AtNRT1.5*/*NPF7.3*, At1g32450), which regulates NO_3^- transfer to Arabidopsis shoots (Lin et al., 2008), and an uncharacterized gene, At3g45700/*NPF2.4*, which was annotated as a proton-dependent oligo-peptide transporter. We prioritized the uncharacterized gene for further study. *NPF2.4* was preferentially expressed in the stele compared to the cortex ($\log_2$ fold change [pericycle versus cortex] = 1.76) and was down-regulated by salt ($\log_2$ fold change 0 mM versus 50 mM = −1.37). A search of the Gene Expression Omnibus Profiles database (Barrett et al., 2013) revealed that *NPF2.4* was rapidly down-regulated in the root after exposure to salt in

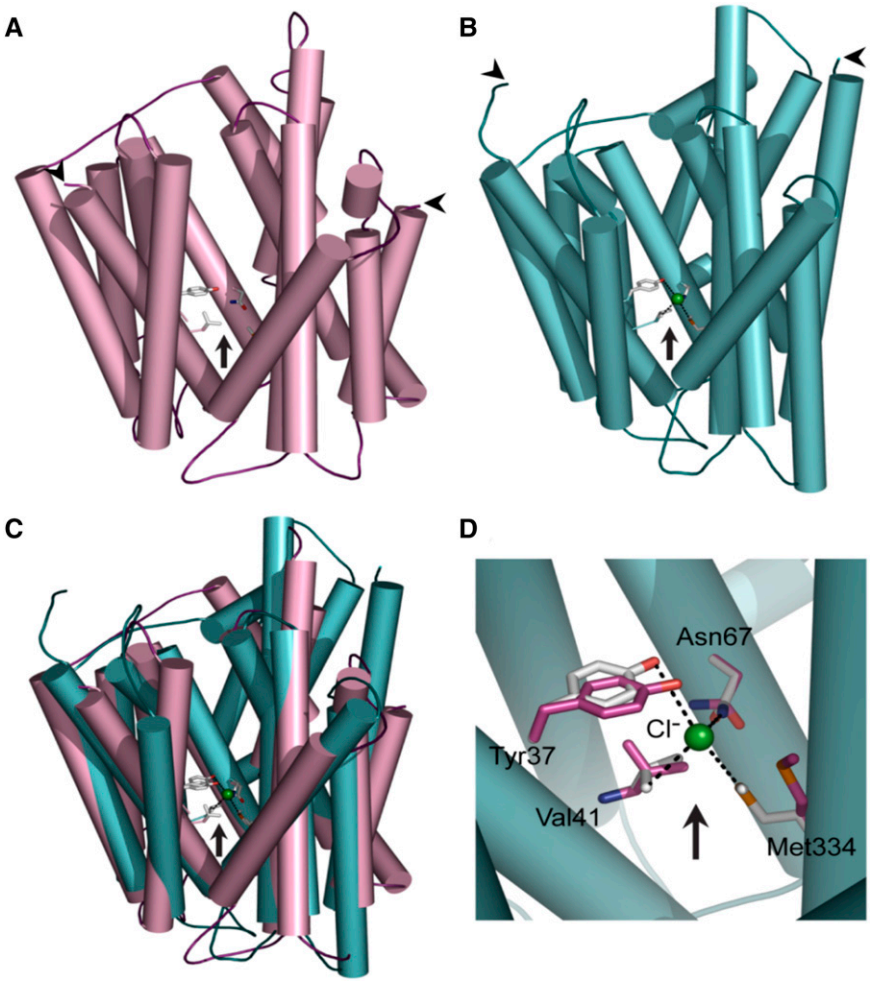

Figure 2. NPF2.4 is likely to form a membrane embedded ion transporter. A 3D homology model of NPF2.4: a proton-dependent oligopeptide transporter from *S. oneidensis* (A; PDB accession 2XUT) and a H^+/NO_3^- transporter from Arabidopsis (B; PDB accession 4OH3) as structural templates. Putative binding site for Cl^- ions is enclosed in a pocket (arrow) and is delineated by four amino acid residues Tyr-37, Val-41, Asn-67, and Met-334, colored in atomic colors. Left and right arrowheads indicate NH_2- and COOH-termini that are predicted to face intracellular sides. C, Superposition of both models showing very similar folds and positions of residues participating in binding of Cl^-. D, A detail of the putative Cl^- binding pocket, signifying residues that are likely to bind Cl^-, and their predicted structural shift upon binding Cl^-. Sticks in magenta and atomic colors indicate residues in the NPF2.5 apo- and Cl^--complexed models, respectively. Dashed lines specify distances between the four binding residues and the Cl^- ion.

other studies (Gene Expression Omnibus accession GDS3216).

Candidate Gene *At3g45700*, Also Known as *NPF2.4*, Is a Member of the *NAXT* Subfamily, a Seven-Gene Clade Belonging to the *NPF* in Arabidopsis

NPF2.4 belongs to the NITRATE EXCRETION TRANSPORTER (*NAXT*) subfamily of the Nitrate Transporter 1/Peptide Transporter (*NRT1/PTR*) family (*NPF*) in Arabidopsis (Segonzac et al., 2007; Tsay et al., 2007; Léran et al., 2014). The *NAXT* subfamily consists of seven genes (*At3g45650*, *At3g45660*, *At3g45680*, *At3g45690*, *At3g45700*, *At3g45710*, and *At3g45720*), which are clustered on chromosome 3 (Fig. 1; Tsay et al., 2007). The *NAXT* subfamily was so named after the properties of *NAXT1/NPF2.7* (*At3g45650*), a NO_3^- transporter in root cortical cells involved in NO_3^- excretion from the root (Segonzac et al., 2007).

In Silica Modeling Suggests *NPF2.4* Is a Membrane-Embedded Transporter That Can Bind Cl^-

The candidate gene *NPF2.4* harbors four exons and three introns and is predicted to encode a 548-amino acid protein, consisting of 12 transmembrane α-helices with a hydrophilic loop between transmembrane α-helices 6 and 7 (Fig. 2). The protein sequence of NPF2.4 was found to have a 64% identity and a 78% similarity to NAXT1/NPF2.7 and a 76% identity and a 85% similarity to NPF2.3, a NO_3^- selective xylem loader in Arabidopsis root (Taochy et al., 2015; Supplemental Fig. S1).

A three-dimensional (3D) molecular model of NPF2.4 was constructed using crystal structures of a proton-dependent oligo-peptide transporter from *Shewanella oneidensis* (PDB accession 2XUT; Fig. 2A; Newstead et al., 2011) and a structure of the NRT1.1/NPF6.3 H^+/NO_3^- transporter from Arabidopsis in complex with a NO_3^- ion (Fig. 2B; Sun et al., 2014). The putative 3D structure of NPF2.4 derived through use of both structural templates indicated the presence of a central cavity, which was common to both structural templates (Fig. 2C). The presence of Cl^- ions could be simulated, and several residues, including Tyr-37, Val-141, Asn-67, and Met-334, were identified in NPF2.4 as important in forming a potential cavity essential for anion transport activity (Fig. 2D). This provides an additional basis for further study of NPF2.4 as a candidate for transporting Cl^- between roots and shoots.

NPF2.4 Expression Is Down-Regulated by Both Salt and ABA

Expression profiling by quantitative RT-PCR (qRT-PCR) indicated that both NaCl and ABA treatment significantly reduced the transcript abundance of *NPF2.4*. The reduction in gene expression was found to

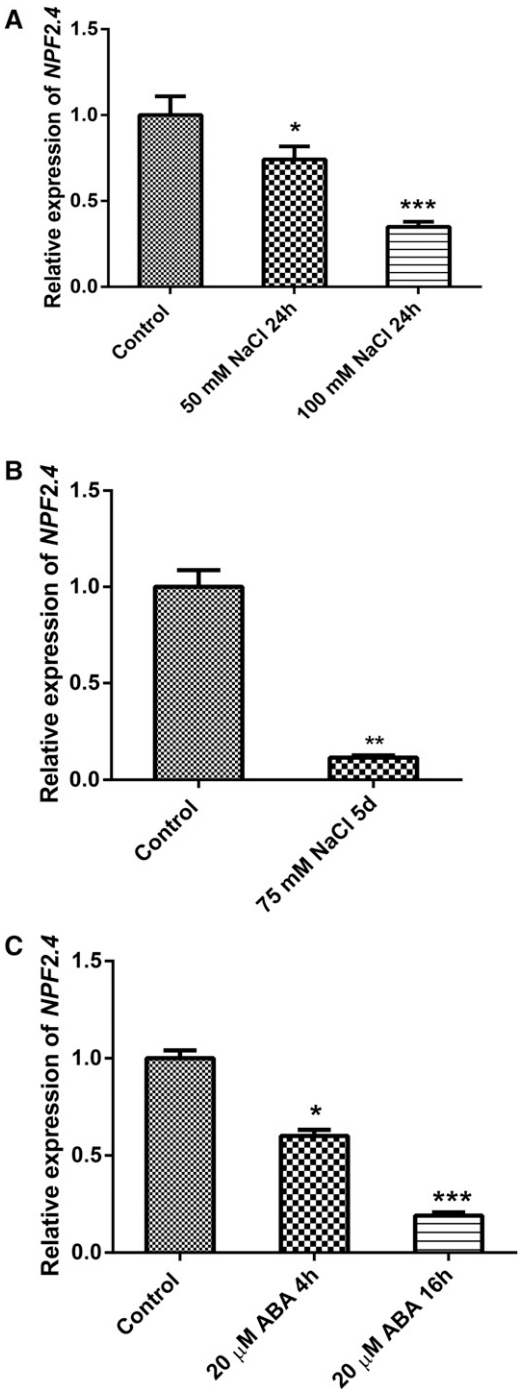

Figure 3. *NPF2.4* expression is down-regulated by both salt and ABA. Four-week-old Col-0 Arabidopsis plants were treated with NaCl or ABA as indicated before their whole roots were harvested for qRT-PCR analysis. A, *NPF2.4* transcripts detected in the root of plants treated with 2 mM (control), 50 mM, or 100 mM NaCl for 24 h. B, *NPF2.4* transcripts detected in the root of plants treated with 2 mM (control) or 75 mM NaCl for 5 d before harvest. C, *NPF2.4* transcripts detected in the root of plants treated with 20 μM +/− cis-,trans-ABA for 4 or 16 h. Results are presented as mean ± SE ($n = 4$ or 5), and expression levels were normalized to controls. Significance is indicated by the asterisks (one-way ANOVA and Tukey test, $^*P \leq 0.05$, $^{**}P \leq 0.01$, and $^{***}P \leq 0.001$).

be concentration dependent, with 100 mM NaCl treatment reducing *NPF2.4* transcript abundance more than 50 mM NaCl (Fig. 3A). When treated with 75 mM NaCl for 5 d, the abundance of *NPF2.4* mRNA in the roots was significantly reduced by almost 90% when compared with untreated plants (2 mM NaCl; Fig. 3B). Exposure to 20 μM ABA for 4 or 16 h significantly reduced *NPF2.4* transcripts in the roots, with the reduction increasing over the time of the assay (Fig. 3C).

NPF2.4 Is Preferentially Expressed in Root Stelar Cells

To examine the localization of *NPF2.4* expression, 1.5 kb of the putative promoter sequence of *NPF2.4* (*proNPF2.4*) was used to drive the expression of the *UidA* reporter gene (Fig. 4). Compared to nontransformed Columbia-0 (Col-0) plants (Fig. 4A), *proNPF2.4*-driven GUS activity was detected in the cells associated with the root vascular bundle in both primary and lateral roots of plants transformed with *proNPF2.4:UidA* (Fig. 4, B–D). GUS activity was also detectible in the vascular cells of both cotyledons and true leaves (Fig. 4, E and F). Transverse sections of 10-d-old *proNPF2.4:UidA*-expressing roots further demonstrated GUS activity in the root stelar cells (Fig. 4G). *ProNPF2.4*-driven GUS activity was also detected in flower and developing siliques (Fig. 4, H and I).

GUS Activity in *proNPF2.4:UidA*-Expressing Plants Is Regulated by Salt, Indicating the Existence of Salt-Responsive Regulatory Elements in the Putative *NPF2.4* Promoter

To investigate the responsiveness of the *NPF2.4* promoter to salt stress, *proNPF2.4:UidA* plants were treated with 75 or 150 mM NaCl for 5 d on Murashige and Skoog (MS) plates. A reduction in the intensity of *proNPF2.4*-associated *GUS* activity was observed

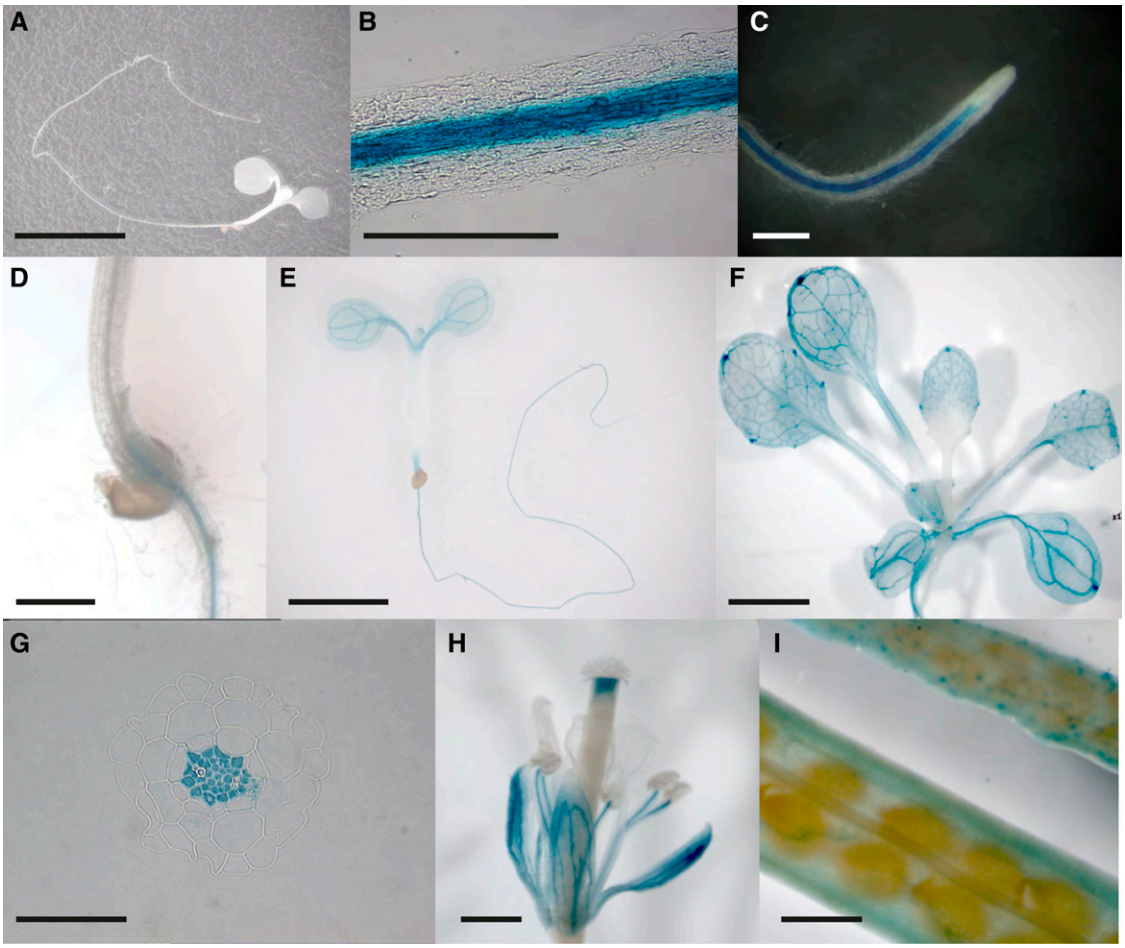

Figure 4. *NPF2.4* is predominantly expressed in the root stelar cells. A, A nontransformed Col-0 plant showing no GUS activity. B and C, Strong *proNPF2.4*-driven GUS activity was detected in the cells associated with mature root stele after 1 h of histochemical staining. D, GUS activity was detected at the root-shoot junction. E and F, GUS activity was detected mainly in the root and the vascular cells in both cotyledon and true leaves. G, Root cross sections prepared from 7-d-old *proNPF2.4:GUS* plants showing GUS activity in the stelar cells. H and I, GUS activity was detected in the flower and siliques.

in response to salt treatments. A fluorescence-based 4-methylumelliferyl-β-galactopyranoside (MUG) assay quantified that *proNPF2.4:UidA* plants treated with 75 or 150 mM NaCl for 5 d had approximately 70% and 30% GUS activity, respectively, when compared with 0 mM NaCl grown plants (Fig. 5).

The 1.5-kb putative promoter region of *NPF2.4* was compared with the entries of the plant cis-acting regulatory DNA elements (PLACE). Multiple copies of binding sites that are targets of transcription factors belonging to ABA signal transduction pathways were identified (Supplemental Table S1).

NPF2.4 Is Localized at the Plasma Membrane

To determine the subcellular localization of NPF2.4, Col-0 plants were stably transformed with *GFP* fused to the 3′-end of *NPF2.4*. GFP was detected on the periphery of root cells in the 10-d-old transgenic plants (Fig. 6A). After plasmolysis was performed to detach the plasma membrane from the cell wall, fluorescence was detected on Hechtian strands (Fig. 6B). To further verify the NPF2.4 localization, *YFP* was fused to the 5′-end of *NPF2.4* and transiently expressed in Arabidopsis mesophyll protoplasts. Figure 6, C to F, shows that *NPF2.4*-associated YFP fluorescence overlapped with the CFP fluorescence of the plasma membrane marker ECFP::Rop11 (Munns et al., 2012).

NPF2.4 Facilitates Cl^- Movement across the Cell Membrane When Expressed in *Xenopus laevis* Oocytes

To test whether NPF2.4 was able to facilitate Cl^- transport, two-electrode voltage clamping of *X. laevis* oocytes injected with *NPF2.4*-cRNA was performed. When the plasma membrane of *NPF2.4*-cRNA injected oocytes was clamped at a negative membrane potential (i.e. that common to plant cells), an inward current was induced in the presence of external Cl^-, which was consistent with the efflux of anions from the oocytes into the extracellular medium through NPF2.4 (Fig. 7A; Supplemental Fig. S2A). To examine whether Cl^- transport activity of NPF2.4 was affected by H^+ concentration (as suggested by the original annotation of NPF2.4 as a proton-dependent oligo-peptide transporter), oocytes were incubated in 50 mM Cl^- at pH values of either 7.5 or 5.5. No pH dependency of the inward current was observed (Fig. 7B; Supplemental Fig. S2, B and C). The magnitude of inward current carried by NO_3^- and Cl^- was compared in *NPF2.4*-injected oocytes and controls, and it was shown that negative currents were much larger and conductance was higher when Cl^- was the external anion, rather than NO_3^- (Fig. 7, C and D; Supplemental Fig. S2, D–G); the P_{Cl-}/P_{NO3-} permeability ratio of NPF2.4 was calculated to be 4.4 ± 0.8 (with either 50 mM NaCl or $NaNO_3$ in the bathing solution). To distinguish whether the observed inward currents at negative membrane potentials were associated with movements of Cl^- or Na^+, oocytes preinjected with *NPF2.4*-cRNA or water were incubated in the solutions having a constant concentration of Na^+ (45 mM) with increasing concentrations of Cl^- (0, 5, 10, 25, and 50 mM), and the inward currents observed were larger when increased Cl^- concentration in the external solution (Fig. 7E; Supplemental Fig. S2, H and I). When using solutions that have a constant concentration of Cl^- (45 mM) with increasing concentrations of Na^+ (0, 5, 10, 25, and 50 mM), similar association between external Na^+ concentrations and the size of inward currents was observed (Fig. 7F; Supplemental Fig. S2, J and K). The effect of different cations on the stimulation of Cl^--carrying currents was examined and found not to be Na^+ specific; K^+ also stimulated Cl^--carrying currents, whereas *N*-Methyl-D-glucamine ($NMDG^+$), Ca^{2+}, and Mg^{2+} did not (Fig. 7G; Supplemental Fig. S2L). When Na^+ was present in the absence of Cl^-, no detectible currents were observed (Fig. 7, A and G; Supplemental Fig. S2L). To test if Na^+ is only activating the transport of Cl^- by NPF2.4, not being cotransported with Cl^-, elemental content of Cl^-, Na^+, and K^+ was measured in both *NPF2.4*-cRNA- and water-injected oocytes incubated in Ca^{2+} ringer solution for 2 d with and without a 2-h low NaCl treatment. *NPF2.4*-cRNA injected oocytes had a significantly lower ($P < 0.001$) Cl^- level compared with water-injected controls. No significant difference was observed in Na^+ content or K^+ content between *NPF2.4*-cRNA injected oocytes and water-injected controls (Fig. 7H). To test whether the observed outward currents at positive membrane potentials (Fig. 7C) were due to Cl^- entering the cell through NPF2.4, a unidirectional $^{36}Cl^-$ influx assay for *NPF2.4*- and water-injected oocytes was performed by incubation in solutions containing 100 mM NaCl or 100 mM NMDG-Cl spiked with low

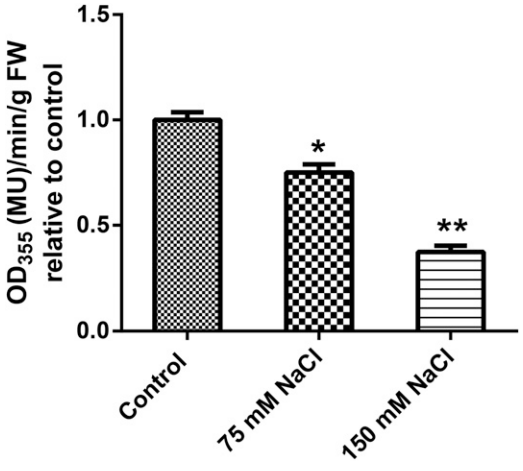

Figure 5. *proNPF2.4*-driven GUS activity in roots is reduced by salt treatments. Two-week-old T2 *proNPF2.4:UidA* plants were GUS stained for 1 h after salt treatments as indicated for 5 d. Roots were subjected to MUG assay. Absorbance measured using a spectrophotometer at 366 mm to measure MUG concentrations. Error bars represent mean ± SE ($n = 3$). Significance is indicated by the asterisks (one-way ANOVA and Tukey test, *$P \leq 0.05$ and **$P \leq 0.01$).

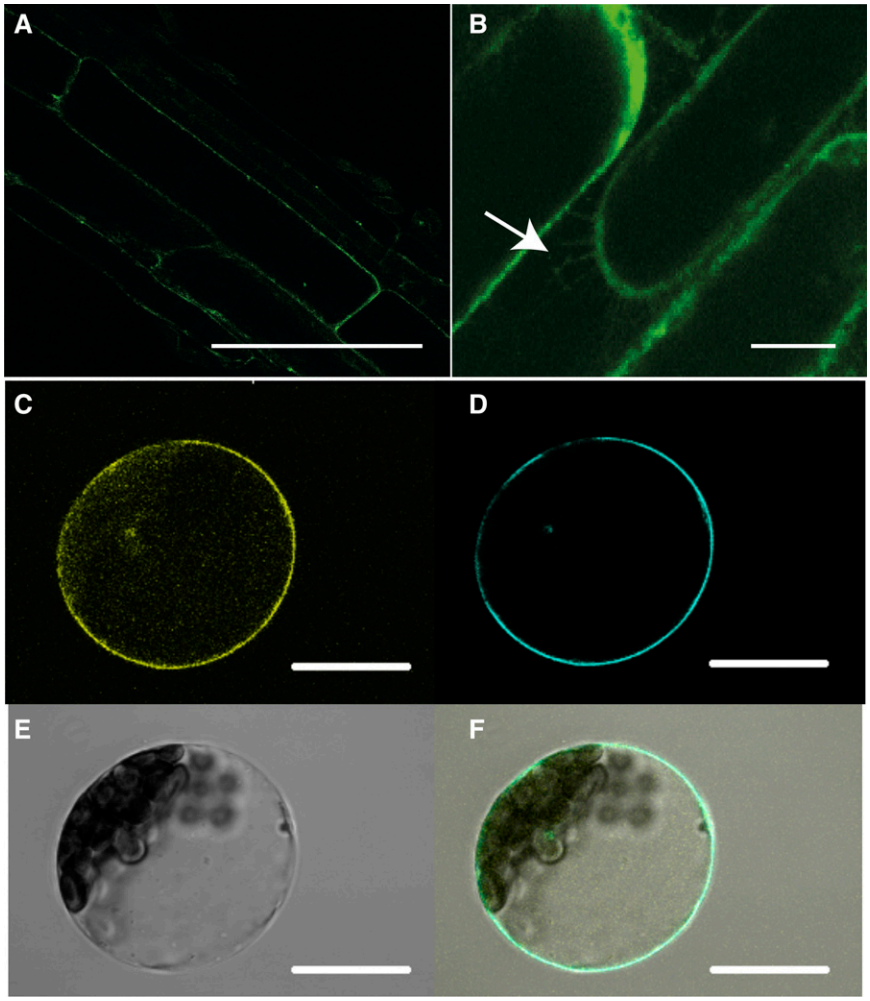

Figure 6. NPF2.4 protein localizes to the plasma membrane. A and B, Constitutive stable expression of *GFP::NPF2.4* in the Arabidopsis root. Bars = 20 μm. A, Confocal image of root cells of 10-d-old *GFP::NPF2.4*-expressing plants showing the plasma membrane localization of GFP tagged NPF2.4. B, Plasmolysis performed on the *GFP::NPF2.4*-expressing plants showing Hechtian strands as indicated by the white arrows. C to E, Transient expression of *YFP::NPF2.4* fusion construct in Arabidopsis mesophyll protoplasts. Bars = 100 μm. C, Confocal image of YFP::NPF2.4 fusion protein in Arabidopsis mesophyll protoplasts. D, Cyan fluorescence of plasma membrane marker ECFP::ROP11. E, Bright-field image of the transformed protoplast. F, Merged image showing the colocalization of YFP::NPF2.4 fusion protein and the plasma membrane marker.

activities of $^{36}Cl^-$ for 60 min (Fig. 7I). Oocytes injected with *NPF2.4*-cRNA exhibited significantly greater uptake of $^{36}Cl^-$ than the water-injected oocytes in presence of NaCl. This stimulated influx was not affected by changes in pH values of 7.5 and 5.5 (Fig. 7I). When NaCl was replaced with NMDG-Cl, there was not a significant increase in the uptake of $^{36}Cl^-$ in *NPF2.4*-cRNA injected oocytes compared to water-injected controls at both pH values tested (Fig. 7I). A unidirectional Na^+ uptake assay, using oocytes incubated in 100 mM NaCl solution spiked with $^{22}Na^+$, confirmed that there was no transmembrane movement of Na^+ through NPF2.4 (Supplemental Fig. S2M).

Knockdown of *NPF2.4* Resulted in Reduced Shoot Cl^- Accumulation

Putative *Atnpf2.4* T-DNA knockouts were ordered from stock centers, but no plants containing an insert within *NPF2.4* and/or lacking *NPF2.4* expression could be identified (Supplemental Fig. S3). Therefore, to elucidate the function of NPF2.4 in planta, artificial microRNAs (amiRNAs) were designed to knock down *NPF2.4* expression. These were transformed into Col-0 plants. qRT-PCR showed that T2 amiRNA plants had 50–80% lower transcript abundance of *NPF2.4* compared with the null segregants (Fig. 8A). These amiRNA plants were shown to have significantly less Cl^- in the shoot when grown under a low salt conditions (2 mM NaCl; 21–32% lower Cl^-; Fig. 8B). Meanwhile, shoot NO_3^- content (Fig. 8C), as well as Na^+ and K^+ (Supplemental Fig. S4, A and B), remained similar between knockdown lines and null segregants. Under a high salt load (75 mM NaCl), when the endogenous *NPF2.4* expression ordinarily decreased in such conditions (Fig. 3B), the transcript abundance of *NPF2.4* in the amiRNA knockdown lines and null segregants was at a similar low level (Supplemental Fig. S4C), and no significant difference in shoot Cl^- concentration was found (Supplemental Fig. S4D). Transcript levels of *NPF2.5*, the closest homolog of *NPF2.4*, were found to be unaffected in the root of *NPF2.4* knockdown lines when compared with null segregants (Supplemental Fig. S4E).

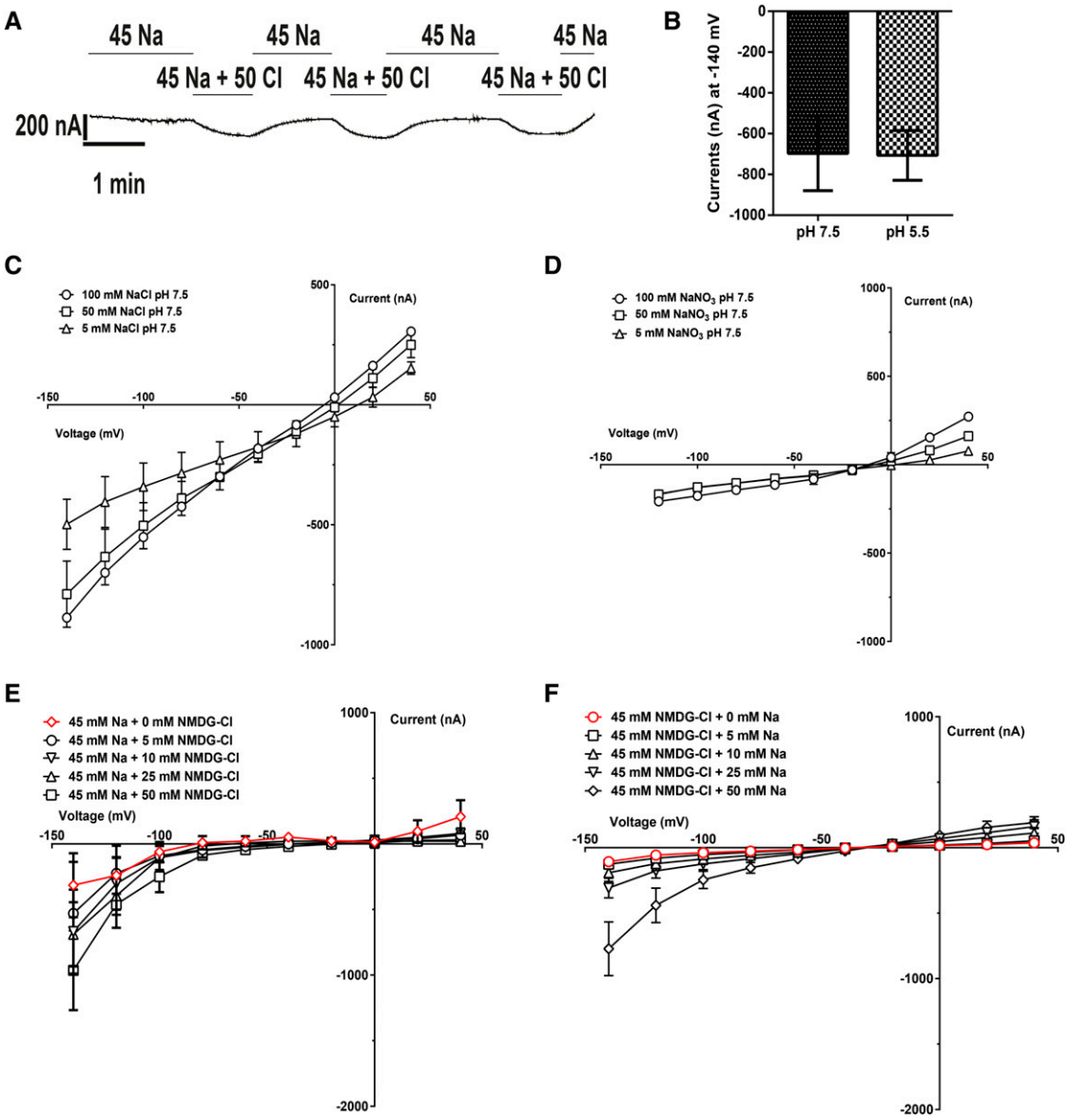

Figure 7. (*Figure continues on following page.*)

Constitutive Overexpression of *NPF2.4* Resulted in Increased Cl^- Accumulation in the Shoot

To investigate the effect of constitutive overexpression of *NPF2.4* on shoot Cl^- accumulation, *NPF2.4* was constitutively overexpressed in Col-0 plants under the control of a *35S* promoter. Two independent T_3 *NPF2.4* overexpression lines were grown for 4 weeks in hydroponics before being exposed to 2 or 75 mM NaCl for 5 d. Greater *NPF2.4* mRNA levels were observed in both *NPF2.4* overexpression lines as detected by qRT-PCR (Supplemental Fig. S5). After the 75 mM NaCl treatment, Cl^- accumulation in the shoot was higher in both overexpression lines compared to the null segregants, with OEX-NPF2.4-2 exhibiting a significant increase of 23% (Fig. 9A). At the same time, no significant difference in shoot content of NO_3^- was found between the transgenic lines and null segregants (Fig. 9B). Small but nonsignificant increases in shoot Cl^- accumulation were observed in *NPF2.4* overexpression lines grown in 2 mM NaCl (Fig. 9C), while no alternation in shoot content of NO_3^- was observed (Fig. 9D).

DISCUSSION

NPF2.4 meets many of the predicted characteristics for a gene encoding an anion channel involved in loading Cl^- to the root xylem. It encodes a protein targeted to the plasma membrane of root stelar cells in Arabidopsis (Figs. 4 and 6), and its expression is strongly down-regulated by salt and ABA treatment

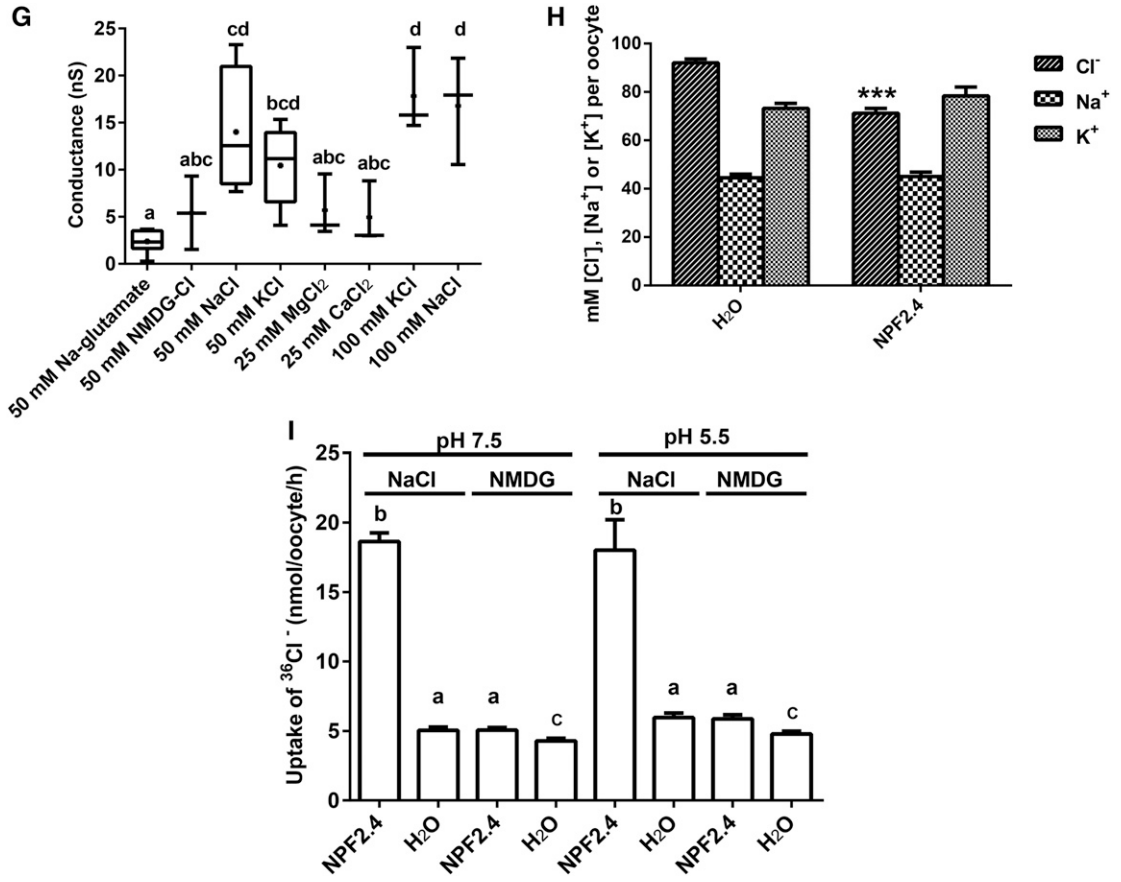

Figure 7. *NPF2.4* generates Na^+- and K^+-dependent Cl^- transport when expressed in *X. laevis* oocytes. *NPF2.4*-cRNA-injected oocytes were exposed to different solutions as indicated. A, Currents over time for *NPF2.4*-cRNA-injected oocytes, 2 d after injection, clamped at –60 mV, in the presence of 45 mM Na-Glu (45 Na) and 45 mM Na-Glu plus 50 mM NMDG-Cl (45 Na + 50 Cl). B, Currents elicited by *NPF2.4*-cRNA when oocytes, held at –140 mV in 50 mM NaCl, were exposed to pH 7.5 or 5.5 ($n = 4$). C, Currents elicited by *NPF2.4*-cRNA when oocytes were exposed to different concentrations of NaCl ($n = 3$). D, Currents elicited by *NPF2.4*-cRNA when oocytes were exposed to different concentrations of $NaNO_3$ ($n = 3$). E, Currents elicited by *NPF2.4*-cRNA when oocytes were exposed to a constant concentration of Na^+ (45 mM) with varying concentrations of Cl^- (0, 5, 10, 25, and 50 mM). F, Currents elicited by *NPF2.4*-cRNA when oocytes were exposed to a constant concentration of Cl^- (45 mM) with varying concentrations of Na^+ (0, 5, 10, 25, and 50 mM). G, Conductance of *NPF2.4*-cRNA-injected oocytes exposed to solutions containing various different ions; conductance was calculated for –80 to –100 mV. Dots are means; maximum and minimum values ± SE are represented by a vertical bar ($n = 3$) or box ($n = 3$–8). Horizontal bars indicate the median; columns with different letters indicate statistically significant differences ($P < 0.05$). H, Concentrations of Cl^-, Na^+, and K^+ measured in the *NPF2.4*-cRNA-injected oocytes and water controls preincubated in Ca^{2+} ringer solution for 2 d. $n = 16$ samples for *NPF2.4*-cRNA-injected oocytes; $n = 10$ samples for water controls; each sample contained 10 oocytes. One-way ANOVA and Tukey test, $^{***}P \leq 0.001$. I, $^{36}Cl^-$ uptake measured in oocytes injected with either *NPF2.4*-cRNA or water, in a background of 100 mM Cl^- for 60 min; results are presented as mean ± SE ($n = 20$); columns with different letters indicate statistically significant differences ($P < 0.05$). B to D and F, Data were plotted after subtraction of currents measured in water-injected oocytes; water-injected control data and total currents in *NPF2.4*-cRNA-injected oocytes are included in Supplemental Figure S2.

(Figs. 3 and 5). *NPF2.4* was found to facilitate Cl^--dependent currents across the cell membrane at negative membrane potentials when expressed in *X. laevis* oocytes (Fig. 7A), and Cl^- transport was not affected by changes in external pH (Fig. 7, B and I). This is consistent with the predicted mechanism of xylem loading for Cl^-, where the difference in electrochemical potential for Cl^- across the plasma membrane of cells in the stele favors passive Cl^- efflux into the xylem, without the need for direct expenditure of energy (Teakle and Tyerman, 2010).

At more positive membrane potentials, the presence of outward currents in *NPF2.4*-injected oocytes indicates that NPF2.4 can also mediate Cl^- influx into cells (Fig. 7C). This was confirmed in *NPF2.4* expressing oocytes using a $^{36}Cl^-$ uptake assay (Fig. 7I). These inwardly directly Cl^- fluxes were dependent, in the conditions tested, upon the presence of Na^+ and were absent when $NMDG^+$ was the balancing cation (Fig. 7I). However, it appears Cl^- transport was not exclusively dependent upon the presence of Na^+, as when K^+ was present but not H^+, Ca^{2+}, Mg^{2+}, or $NMDG^+$, there were

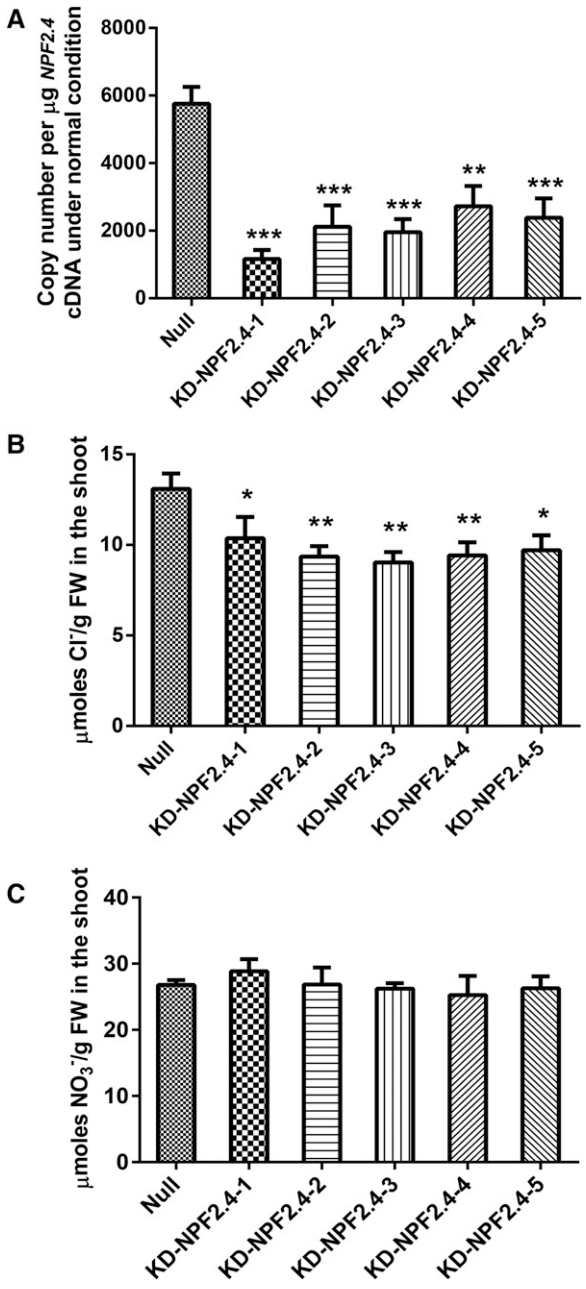

Figure 8. Shoot Cl^- concentration was significantly reduced in the *NPF2.4* amiRNA knockdowns under low salt conditions (2 mM NaCl), whereas the shoot NO_3^- concentration of the *NPF2.4* knockdowns was similar to null segregants. Four-week-old hydroponically grown plants were treated with 2 mM NaCl for 5 d. A, *NPF2.4* expression in the roots of *NPF2.4* knockdowns. B, Cl^- concentrations in the shoot of *NPF2.4* knockdowns and null segregants. C, Shoot NO_3^- concentrations of *NPF2.4* knockdowns and null segregants. Results are presented as mean ± SE, $n = 4$ to 7. Significance is indicated by the asterisks (one-way ANOVA and Tukey test, * $P \leq 0.05$, ** $P \leq 0.005$, and *** $P \leq 0.001$).

also significant Cl^--dependent currents (Fig. 7, F and G). Only Cl^- concentration differences and not Na^+ or K^+ were detected in *NPF2.4*-injected oocytes (Fig. 7H), and no inwardly directed Na^+ fluxes were detected (Supplemental Fig. S2M). These data indicate that both monovalent cations K^+ and Na^+ are likely to activate Cl^- transport but not be carried by NPF2.4, and it is likely that the in vivo activating cation is K^+ in low salt conditions. Under high salt (NaCl) conditions, currents carried by NPF2.4 are likely to be minimized by the lower expression levels of *NPF2.4* despite a higher concentration of another activating cation. Interestingly, the transport properties of NPF2.4 appear to be specific to Cl^-, with no indication of the protein being involved in NO_3^- transport (Fig. 7, C and D), which is unique when compared with other published NPF2s that are generally permeable to NO_3^- (Segonzac et al., 2007; Tsay et al., 2007; Léran et al., 2014). Combining all evidence, it is suggested that, at negative membrane potentials, NPF2.4 facilitates Cl^- efflux across cell membranes, consistent with its proposed role in facilitating a component of the loading of Cl^- into the xylem in Arabidopsis.

The use of transgenic plants demonstrated that altering levels of *NPF2.4* expression could affect shoot Cl^- accumulation but not that of NO_3^-, Na^+, and K^+ (Figs. 8F and 9, B and D; Supplemental Fig. S4, A and B). This ion profile provides further evidence that Na^+ and K^+ are not transported by NPF2.4. Reduction in expression of *NPF2.4* in Arabidopsis using amiRNA resulted in decreased Cl^- accumulation in the shoot (Fig. 8, A and B; Supplemental Fig. S4A), while *NPF2.4* overexpression resulted in increased shoot Cl^- content (under high salt conditions; Fig. 9, A and C), thus indicating a role for NPF2.4 in the accumulation of Cl^- in Arabidopsis shoots. The increased Cl^- accumulation in *NPF2.4* overexpression lines was not significant in low salt conditions (Fig. 9C). Møller et al. (2009) previously observed that the loss of cell specificity when constitutively overexpressing *AtHKT1;1* may not in all conditions lead to an expected change in ion profile, with the use of gene knockouts or cell-specific complementation being more reliable. In this study, amiRNA knockdown was performed to lend a greater cell type specificity when manipulating expression of *NPF2.4*. Reducing expression of *NPF2.4* by 80% under a low salt condition (2 mM NaCl), without affecting the expression of genes that are homologous to *NPF2.4*, resulted in a decrease in the shoot accumulation of Cl^- by up to 31% when compared with the null segregants (Fig. 8, A and B; Supplemental Fig. S4E); however, this was insufficient to account for a measurable difference in growth (Supplemental Fig. S6). Due to the nature of the amiRNA system, knocking down the expression of *NPF2.4* does not completely remove its transcript, thus still leaving small amounts of *NPF2.4* mRNA that can be translated into a functioning protein. Unfortunately no lines with *NPF2.4* completely knocked out could be identified to test whether a lack of *NPF2.4* expression resulted in a greater reduction of shoot Cl^-. Under high salt conditions (75 mM NaCl), the endogenous down-regulation of *NPF2.4* expression (Fig. 3) resulted in similar levels of *NPF2.4* expression in both knockdowns and null segregants (Supplemental Fig. S4C); thus, as

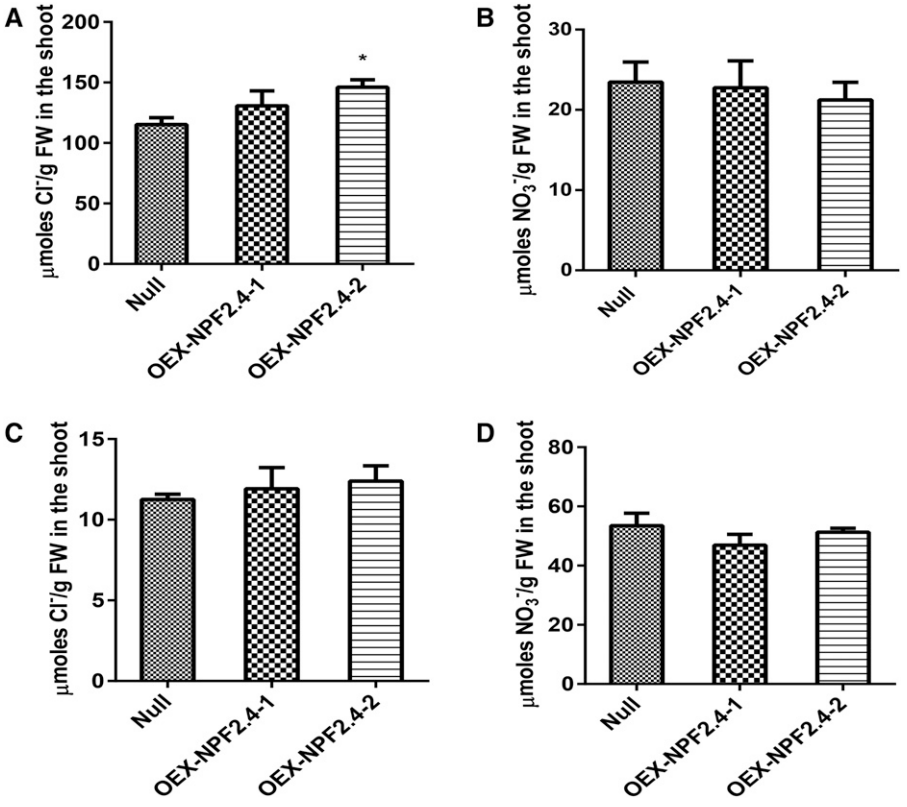

Figure 9. Shoot accumulation of Cl^- was increased in the *NPF2.4* overexpression lines, while NO_3^- content remained unaffected. A, Cl^- concentrations in the shoot of *NPF2.4* overexpression lines and null segregants after high salt treatment (75 mM NaCl). B, NO_3^- concentrations in the shoot of *NPF2.4* overexpression lines and null segregants after high salt treatment. C, Cl^- concentrations in the shoot of *NPF2.4* overexpression lines and null segregants after low salt treatment (2 mM NaCl). D, NO_3^- concentrations in the shoot of *NPF2.4* overexpression lines and null segregants after low salt treatment. Error bars represent mean ± SE; $n = 4$. Significance is indicated by the asterisks (single-factor ANOVA and Tukey test, * $P \leq 0.05$).

expected, no difference in shoot Cl^- concentration was found (Supplemental Fig. S4D).

Cl^- xylem loading is a complex process, as revealed by at least three anion conductances identified in stelar protoplasts (Köhler and Raschke, 2000; Gilliham and Tester, 2005). The electrophysiological profiles of NPF2.4 in *X. laevis* oocytes did not resemble X-QUAC, the likely major conductance for Cl^- loading into the xylem. First, there was a lack of rectification (Fig. 7C). This suggests the involvement of other transport proteins and/or regulators in the loading of Cl^- into the xylem (Roy et al., 2008; Henderson et al., 2014). Furthermore, *NPF2.4*-induced currents in oocytes were considerably smaller in the presence of NO_3^- compared to Cl^- (Fig. 7, C and D), whereas X-QUAC type currents were much more permeable to NO_3^- compared to Cl^- (Köhler and Raschke, 2000; Gilliham and Tester, 2005). From the plant data it is clear that NPF2.4 is not the only transporter that facilitates the loading of Cl^- into the transpiration stream. Shoot Cl^- is reduced by 31% relative to controls, and shoot NO_3^- remains unchanged when there is an 80% reduction in *NPF2.4* expression in the amiRNA lines indicating that other mechanisms contribute to the remaining Cl^- loading (Fig. 8, A and B). There are other anion transporters in Arabidopsis that may contribute to Cl^- net xylem loading, some of which contribute to NO_3^- loading, such as NRT1.5/NPF7.3 and NRT1.8/NPF7.2 (Lin et al., 2008; Li et al., 2010), and SLAH1, a root-stelar specific homolog of SLAC1 (a protein responsible for Cl^- efflux from guard cells and its homolog SLAH3; Negi et al., 2008; Vahisalu et al., 2008), and a cation-Cl^- cotransporter (Colmenero-Flores et al., 2007; Henderson et al., 2015). Interestingly, *NRT1.5/NPF7.3* and *NRT1.8/NPF7.2* were shown to be down- and up-regulated, respectively, by salt stress, with *nrt1.5/npf7.3* knockout plants exhibiting improved salinity tolerance (Lin et al., 2008; Li et al., 2010; Chen et al., 2012). The involvement of NRT and SLAH proteins in Cl^- transport has not yet been reported.

The reduction in *NPF2.4* expression after the application of ABA and the suggestion of ABA's role in regulating Cl^- transport from the root to the shoot warrants further study. ABA is a signal known to down-regulate Cl^- loading of the shoot and the conductances that are responsible for this flux (Cram and Pitman, 1972; Gilliham and Tester, 2005), whereas in stomatal guard cells, ABA activates Cl^- efflux from cells (Negi et al., 2008; Vahisalu et al., 2008; Geiger et al., 2009; Lee et al., 2009; Vahisalu et al., 2010). Therefore, it will be interesting to explore the differences in ABA signaling pathways for these processes that differentially regulate anion efflux from root and shoot cells.

The Cl^- transport activity of NPF2.4 observed in this study adds to the list of solutes transported by members of the NPF. To date, NO_3^-, dipeptides, histidine, malate, glucosinolate, auxin, and ABA have been reported as substrates transported by various NPFs (Yamashita et al., 1997; Zhou et al., 1998; Jeong et al., 2004; Krouk et al., 2010; Kanno et al., 2012; Nour-Eldin et al., 2012). The increasing volume of genomic and functional evidence on the roles of the NPF will assist in addressing the question posed by Tsay et al. (2007) as to why plants

have so many NPF genes (53 in Arabidopsis and 80 in rice), while yeast, *Drosophila melanogaster*, and humans have only one, three, and six members, respectively. NPF transporters identified from organisms other than higher plants are di-/tripeptide transporters; therefore, it was speculated that the NO_3^- transport activity of this family in Arabidopsis has evolved from an ancient peptide transporter (Stacey et al., 2002; Tsay et al., 2007). Since then, the NPF family has expanded, presumably to fill specific transport roles in specific environments, making it increasingly diverse.

In conclusion, NPF2.4 is a protein involved in Cl^- xylem loading in Arabidopsis, regulating Cl^- accumulation in the shoot in response to salt stress. To our knowledge, the identification and functional characterization of NPF2.4 has, for the first time, revealed the molecular properties of a protein that loads Cl^- into the xylem. As such, *NPF2.4* may be a target for improving plant salinity tolerance in crops that are sensitive to Cl^- accumulation. Further research is needed to investigate whether *NPF2.4* orthologs are involved in salinity tolerance in other plant species and whether manipulation of *NPF2.4-like* genes and other genes involved in Cl^- transport to the shoot of crop plants is important for alleviating Cl^- toxicity.

MATERIALS AND METHODS

Plant Material and Growth Conditions

Plant Material

T-DNA knockout lines (SALK_111056 and SALK_111071), which were annotated with the T-DNA site of insertion being in the *NPF2.4* gene, as well as Col-0 Arabidopsis seeds were obtained from the European Arabidopsis Stock Centre.

Soil-Grown Arabidopsis

Arabidopsis (*Arabidopsis thaliana*) was grown in soil prepared following the methods described by Møller et al. (2009). Plants were kept with light/dark photoperiods of either 16 h/8 h (long-day) or 10 h/14 h (short-day). Temperature was maintained between 21°C and 23°C; humidity was optimized between 60% and 75%; photon irradiance at the level of plant the leaves was approximately 120 μmol m^{-2} s^{-1}.

Hydroponics-Grown Arabidopsis

Arabidopsis plants were germinated and grown in hydroponics following the method described by Conn et al. (2013). Growth conditions were similar to those for soil-grown plants. At the time of salt application, NaCl solutions of different concentrations as indicated in the text were applied to the growth solution 4 weeks after germination with supplemental Ca^{2+} added.

Expression Analysis

Gene expression analysis by qRT-PCR was performed following the method described by Burton et al. (2008). The primers for determining *NPF2.4* expression were 5′-CAGAAGCTAATCCGCAAACC-3′ (forward) and 5′-AGGAACCAGCCATAGCACTG-3′ (reverse). The selected control genes and data normalizations followed the protocols described by Jha et al. (2010).

Phylogenetic Analysis

Multiple amino acid sequence alignment was performed with ClustalW2. Proteins used in the alignment included characterized Arabidopsis NPFs and seven members of the NAXT subfamily, as shown in the table below. Protein sequences were retrieved from the Arabidopsis genome annotation database release 9 (http://www.arabidopsis.org/). The neighbor-joining phylogenetic tree was generated using Mega5, with 5000 bootstrap iterations (Tamura et al., 2011).

Protein 3D Structural Modeling

The 3D models of NPF2.4 were constructed and evaluated as described by Cotsaftis et al. (2012) using two structural templates: (1) a proton-dependent oligopeptide transporter from *Shewanella oneidensis* (Newstead et al., 2011; PDB accession 2XUT) and (2) a NO_3^- transporter from Arabidopsis in complex with the NO_3^- ion (Sun et al., 2014; PDB accession 4OH3). The amino acid sequences of 2XUT (488 residues) and 4OH3 (553 residues, NO_3^- ion replaced by Cl^- ion) were aligned with NPF2.4 (503 and 528 residues) using the Local Meta-Threading Server (Wu and Zhang, 2007), Alignment Annotator (Gille et al., 2014), followed by manual alignment adjustments. The aligned sequences were used as input parameters to generate 3D models of NPF2.4 using modeler 9v8 (Sali and Blundell, 1994) on a Linux station, running the Fedora 12 operating system. Three types of 3D models (using 2XUT or 4OH3 as the templates, the latter with and without Cl^-) were selected from 40 models based on their low value of the modeler 9v8 objective function and the most favorable DOPE energy scoring parameters (Shen and Sali, 2006). Images of structural models were generated in the PyMol Molecular Graphics System, version 1.3 (Schrödinger LLC).

Generation of *NPF2.4* Overexpression Lines and *NPF2.4* AmiRNA Knockdown Lines

AmiRNA NPF2.4

A Web microRNA designer (http://wmd2.weigelworld.org/cgi-bin/mirnatools.pl; Schwab et al., 2006) was used to design two amiRNA constructs to knock down *NPF2.4* gene expression. Two 21-bp target sequences were identified from the *NPF2.4* coding sequence, allowing the generation of two independent amiRNA constructs. A set of primers (Supplemental Table S2) was used to incorporate the 21-bp amiRNA sequence into the MIR319a vector (Schwab et al., 2006). The amiRNA constructs then were cloned into *pCR8* and transferred to *pTOOL2* (Roy et al., 2013) by an LR reaction (Invitrogen) and transformed into Arabidopsis Col-0 plants using *Agrobacterium tumefaciens*-mediated transformation (Clough and Bent, 1998; Weigel and Glazebrook, 2002).

35S:NPF2.4

cDNA of NPF2.4 was amplified using Platinum Taq (Invitrogen) and cloned into Gateway-enabled pCR8 entry vector (Invitrogen). NPF2.4 was transferred from pCR8 to the pTOOL2 destination vector (Roy et al., 2013) using LR Clonase II (Invitrogen) and transformed into Arabidopsis Col-0 plants using *Agrobacterium*-mediated floral dip transformation (Clough and Bent, 1998; Weigel and Glazebrook, 2002).

Promoter GUS Fusions

The primers 5′-TAGAGAAGAAGACTATCATGGG-3′ (forward) and 5′-GGAGGTACTTTGACTTGTGTTTGAG-3′ (reverse) were used to amplify 1.5 kb of the sequence upstream from the start codon of *NPF2.4*. This fragment was cloned into *pCR8* and transferred by LR reaction into *pMDC162* to drive *UidA* expression. The destination vector was transformed into Arabidopsis Col-0 plants using the *Agrobacterium*-mediated method (Clough and Bent, 1998; Weigel and Glazebrook, 2002). Two-week-old T2 *proNPF2.4:UidA* plants were stained for GUS activity for 1 h following the protocol described by Weigel and Glazebrook (2002). GUS activity was visualized using a Leica MZ16FA stereo microscope (Leica Microsystems). To prepare transverse sections of roots of *proNPF2.4:UidA* plants, GUS-stained material was washed with milliQ water and fixed at 4°C overnight using 0.1 M phosphate buffer with 5% glutaraldehyde. Samples were washed twice with 1× PBS for 10 min each and embedded in 1% agarose. Tissue was dehydrated by 15-min incubations in an ethanol series of 50, 70, 90, and 100% (v/v). Samples were transferred to Technovit 7100 hydroxyethyl methacrylate resin solution with 2.5% (v/v) PEG400 and polymerized in thin-walled PCR tubes. Eight-micrometer-thick transverse root

sections were cover slipped in DPX mountant and imaged on a Leica ASLMD compound microscope equipped with a DFC480 CCD camera.

To test the effect of the salt treatments on GUS activity, *proNPF2.4:UidA* plants were grown vertically on 0.5× MS media for 7 d before transferred onto 0.5× MS media containing 0, 75, or 150 mM NaCl for a 5-d salt treatment. Salt-treated plants were GUS stained for 1 h and examined under a Leica MZ16FA stereomicroscope (Leica Microsystems). A fluorescent MUG assay was performed to quantify the GUS activity of *proNPF2.4:UidA* plants after the salt treatments following the protocol described by Peña (2004).

NPF2.4::GFP Fusion Constructs and Visualization of Fluorescence in Planta

To determine the subcellular localization of NPF2.4 in planta, *GFP6* was fused to either the 5′- and 3′-end of *NPF2.4* and used for constructing *GFP::NPF2.4* and *NPF2.4::GFP*. The coding sequence of *NPF2.4* was inserted into the destination vectors *pMDC44* and *pMDC83* (Curtis and Grossniklaus, 2003) to generate the necessary vectors. The fusion vectors were transformed into Arabidopsis Col-0 plants using an *Agrobacterium*-mediated method (Clough and Bent, 1998; Weigel and Glazebrook, 2002). T2 transgenic plants were geminated on 0.5× MS media under hygromycin selection. Ten days after the germination, plants were stained with 10 μg/mL propidium iodide for 5 min and rinsed with deionized water. Plasmolysis was conducted on a slide by applying 10% (w/v) Suc solution on to the roots of *GFP6*-expressing plants. GFP (excitation, 488 nm; emission, 505–530 nm) and propidium iodide (PI) (excitation, 543 nm; emission long-pass, 560 nm) fluorescence were visualized using a LSM5 PASCAL laser scanning microscope (Carl Zeiss) running PASCAL imaging software (version 3.2 SP2; Carl Zeiss).

Arabidopsis Mesophyll Cell Transient Transformation

To determine the subcellular localization of NPF2.4 in Arabidopsis protoplasts, *YFP* was fused to the 5′-end of *NPF2.4* by cloning the coding sequence of *NPF2.4* into the destination vector *pattR-YFP* (Subramanian et al., 2006). A protein known to be targeted to the plasma membrane (ROP11) was used as a positive control (eCFP::ROP11; Molendijk et al., 2008). Protoplast isolation from Arabidopsis mesophyll cells and polyethylene glycol-mediated transient transformation were conducted using the protocols described by Yoo et al. (2007) to introduce the fusion vector. CFP (excitation, 436 nm; emission, 470–535 nm) and YFP (excitation, 514 nm; emission, 525–610 nm) fluorescence was visualized using a LSM5 PASCAL laser scanning microscope running PASCAL imaging software (version 3.2 SP2).

Electrophysiology

Two-Electrode Voltage Clamping

A *pGEMHE-DEST* destination vector (Shelden et al., 2009) was developed for heterologous expression of *NPF2.4* in *Xenopus laevis* oocytes. cRNA was transcribed from this vector using the mMESSAGE mMACHINE kit (Ambion) following the manufacturer's instructions and injected into the following (Munns et al., 2012). Two-electrode voltage clamping was performed following Roy et al. (2008). Osmolarities of all solutions were adjusted using mannitol (Sigma) to 240–260 mOsmol/kg (Fiske 210 Micro-Sample Osmometer; Advanced Instruments). Membrane currents were recorded in solutions containing 5 mM MES, 2 mM Ca-gluconate ± NMDG-Cl (or NaCl), or NMDG-NO_3 (or $NaNO_3$) as indicated. Data were acquired and analyzed using pClamp 8.2 (Axon Instruments). Experiments were repeated using oocytes harvested from different *X. laevis* surgeries.

Isotope Uptake Assay ($^{36}Cl^-$ and $^{22}Na^+$)

X. laevis oocytes microinjected with either *NPF2.4* cRNA or water were prepared for $^{36}Cl^-$ and $^{22}Na^+$ uptake. Oocytes were incubated in Cl^--free ND96 media (96 mM sodium isethionate, 2 mM potassium gluconate, 1.8 mM calcium gluconate, 1 mM magnesium gluconate, 5 mM HEPES, 2.5 mM sodium pyruvate, and 5% gentamycin, pH 7.4) for 120 min 2 d after injection. Oocytes were then incubated in uptake buffer (100 mM NaCl, 2 mM Ca-gluconate, 2 mM K-gluconate, 5 mM MES, and 240 mOsmol kg^{-1} water, pH 7.5) supplemented with 1 μCi/mL of $Na^{36}Cl$ (Radiochemical Centre Limited) or 2 μCi/mL $^{22}NaCl$ (Perkin-Elmer) for 1 h. The oocytes were washed twice with ice-cold uptake buffer, which did not contain $^{36}Cl^-$ or $^{22}Na^+$, and each individual oocyte transferred into 1.5-mL microcentrifuge tubes containing 20 μL of 0.1 M nitric acid and macerated by pipetting or transferred to scintillation vials containing 200 μL of 10% SDS and left overnight. Four milliliters of scintillation fluid was added to each scintillation vial. Radioactivity, counts per minute, of $^{36}Cl^-$ or $^{22}Na^+$ was measured using a Tri-Carb liquid scintillation counter (Perkin-Elmer) or a Beckman Coulter LS6500 scintillation counter.

Elemental Analysis of Cl^-, Na^+, K^+, and NO_3^-

Concentration of Cl^-, Na^+, K^+, and NO_3^- was determined in the whole shoot of Arabidopsis seedlings. The shoot was weighed, freeze-dried, and ground into a powder. To determine Arabidopsis shoot and *X. laevis* oocyte Cl^- concentrations, approximately 10 to 20 mg of material was digested in 2 mL of 1% nitric acid at 80°C overnight and 10 oocytes were digested in 1 mL of 1% nitric acid at 75°C for 2 h. Cl^- content was analyzed using a chloride analyzer (Sherwood Scientific model 926) following the manufacturer's instructions. The NO_3^- assay described by Kamphake et al. (1967) was used for the determination of the NO_3^- concentration in plant tissue. To examine Na^+ and K^+ in plants or oocytes, the youngest fully expanded leaf or incubated oocytes were harvested and digested in 1% nitric acid at 80°C overnight for plant tissues or 75°C for 2 h for oocytes following Byrt et al. (2014). Samples were diluted and measured relative to appropriate standard solutions using a model 420 flame photometer (Sherwood Scientific).

Accession Numbers

Sequence data from this article can be found in the GenBank/EMBL data libraries under accession number NM_114439.

Supplemental Data

The following supplemental materials are available.

Supplemental Figure S1. Multiple sequence alignment of NPF2.4, NPF2.3, and NPF2.1/ NAXT1.

Supplemental Figure S2. Raw and control data for expression of NPF2.4 in *Xenopus laevis* oocytes.

Supplemental Figure S3. *NPF2.4* transcript levels of lines SALK_111056 and SALK_111071 annotated as T-DNA knockouts for *NPF2.4* showed the failed disruption of *NPF2.4* expression in both lines.

Supplemental Figure S4. Under low salt condition, shoot concentration of both Na^+ and K^+ were similar between *NPF2.4* knockdowns and null segregants.

Supplemental Figure S5. Expression validation of *NPF2.4* in the root of *NPF2.4* overexpression lines under both low salt and high salt conditions.

Supplemental Figure S6. Biomass of *NPF2.4* knockdowns was unaffected by low salt condition compared to null segregants.

Supplemental Table S1. The ABA signaling pathway associated cis-acting elements in the putative promoter region of *NPF2.4*.

Supplemental Table S2. Primers used for the generation of *NPF2.4*-amiRNA constructs.

ACKNOWLEDGMENTS

We thank Andrew Jacobs for the destination vectors used in this study, Yuan Li for performing the qRT-PCRs (Australian Centre for Plant Function Genomics), Steven Tyerman and Sunita Ramesh (University of Adelaide) for the aid with the electrophysiology experiments, Detlef Weigel (Max Planck Institute for Developmental Biology, Tübingen, Germany) for providing pRS300 plasmid for the generation of amiRNA constructs, and Christina Morris for editing English language of this manuscript.

Received July 29, 2015; accepted December 4, 2015; published December 11, 2015.

LITERATURE CITED

Abel GH (1969) Inheritance of the capacity for chloride inclusion and chloride exclusion by soybeans. Crop Sci **9:** 697–698

Apse MP, Blumwald E (2007) Na^+ transport in plants. FEBS Lett **581:** 2247–2254

Barrett T, Wilhite SE, Ledoux P, Evangelista C, Kim IF, Tomashevsky M, Marshall KA, Phillippy KH, Sherman PM, Holko M, et al (2013) NCBI GEO: archive for functional genomics data sets–update. Nucleic Acids Res **41:** D991–D995

Bassil E, Blumwald E (2014) The ins and outs of intracellular ion homeostasis: NHX-type cation/$H(^+)$ transporters. Curr Opin Plant Biol **22:** 1–6

Beilby MJ, Walker NA (1981) Chloride transport in *Chara*: I. Kinetics and current-voltage curves for a probable proton symport. J Exp Bot **32:** 43–54

Berthomieu P, Conéjéro G, Nublat A, Brackenbury WJ, Lambert C, Savio C, Uozumi N, Oiki S, Yamada K, Cellier F, et al (2003) Functional analysis of AtHKT1 in Arabidopsis shows that $Na(^+)$ recirculation by the phloem is crucial for salt tolerance. EMBO J **22:** 2004–2014

Burton RA, Jobling SA, Harvey AJ, Shirley NJ, Mather DE, Bacic A, Fincher GB (2008) The genetics and transcriptional profiles of the cellulose synthase-like *HvCslF* gene family in barley. Plant Physiol **146:** 1821–1833

Byrt CS, Platten JD, Spielmeyer W, James RA, Lagudah ES, Dennis ES, Tester M, Munns R (2007) HKT1;5-like cation transporters linked to Na^+ exclusion loci in wheat, *Nax2* and *Kna1*. Plant Physiol **143:** 1918–1928

Byrt CS, Krishnan M, Xu B, Lightfoot D, Athman A, Watson-Haigh NS, Jacobs A, Plett D, Munns R, Tester M, Gilliham M (2014) Accumulation of Na^+ in bread wheat is controlled by the Na^+ transporter TaHKT1; 5-D. Plant J **80:** 516–526

Chen C-Z, Lv X-F, Li J-Y, Yi H-Y, Gong J-M (2012) Arabidopsis NRT1.5 is another essential component in the regulation of nitrate reallocation and stress tolerance. Plant Physiol **159:** 1582–1590

Clough SJ, Bent AF (1998) Floral dip: a simplified method for *Agrobacterium*-mediated transformation of *Arabidopsis thaliana*. Plant J **16:** 735–743

Cole PJ (1985) Chloride toxicity in citrus. Irrig Sci **6:** 63–71

Colmenero-Flores JM, Martínez G, Gamba G, Vázquez N, Iglesias DJ, Brumós J, Talón M (2007) Identification and functional characterization of cation-chloride cotransporters in plants. Plant J **50:** 278–292

Conn SJ, Hocking B, Dayod M, Xu B, Athman A, Henderson S, Aukett L, Conn V, Shearer MK, Fuentes S, Tyerman SD, Gilliham M (2013) Protocol: optimising hydroponic growth systems for nutritional and physiological analysis of *Arabidopsis thaliana* and other plants. Plant Methods **9:** 4

Cotsaftis O, Plett D, Shirley N, Tester M, Hrmova M (2012) A two-staged model of Na^+ exclusion in rice explained by 3D modeling of HKT transporters and alternative splicing. PLoS One **7:** e39865

Cram W, Pitman M (1972) The action of abscisic acid on ion uptake and water flow in plant roots. Aust J Biol Sci **25:** 1125–1132

Curtis MD, Grossniklaus U (2003) A Gateway cloning vector set for high-throughput functional analysis of genes *in planta*. Plant Physiol **133:** 462–469

Davenport RJ, Muñoz-Mayor A, Jha D, Essah PA, Rus A, Tester M (2007) The Na^+ transporter AtHKT1;1 controls retrieval of Na^+ from the xylem in *Arabidopsis*. Plant Cell Environ **30:** 497–507

Evrard A (2013) Cell type-specific transcriptional responses of plants to salinity. University of Adelaide, Adelaide, Australia

Evrard A, Bargmann BR, Birnbaum K, Tester M, Baumann U, Johnson AT (2012) Fluorescence-activated cell sorting for analysis of cell type-specific responses to salinity stress in Arabidopsis and rice. *In* S Shabala, TA Cuin, eds, Plant Salt Tolerance, **Vol 913**. Humana Press, New York, pp 265–276

Felle HH (1994) The H^+/Cl^- symporter in root-hair cells of *Sinapis alba* (an electrophysiological study using ion-selective microelectrodes). Plant Physiol **106:** 1131–1136

Gaymard F, Pilot G, Lacombe B, Bouchez D, Bruneau D, Boucherez J, Michaux-Ferrière N, Thibaud JB, Sentenac H (1998) Identification and disruption of a plant shaker-like outward channel involved in K^+ release into the xylem sap. Cell **94:** 647–655

Geiger D, Scherzer S, Mumm P, Stange A, Marten I, Bauer H, Ache P, Matschi S, Liese A, Al-Rasheid KAS, Romeis T, Hedrich R (2009) Activity of guard cell anion channel SLAC1 is controlled by drought-stress signaling kinase-phosphatase pair. Proc Natl Acad Sci USA **106:** 21425–21430

Geilfus C-M, Mithöfer A, Ludwig-Müller J, Zörb C, Muehling KH (2015) Chloride-inducible transient apoplastic alkalinizations induce stomata closure by controlling abscisic acid distribution between leaf apoplast and guard cells in salt-stressed *Vicia faba*. New Phytol **208:** 803–816

Gille C, Birgit W, Gille A (2014) Sequence alignment visualization in HTML5 without Java. Bioinformatics **30:** 121–122

Gilliham M, Tester M (2005) The regulation of anion loading to the maize root xylem. Plant Physiol **137:** 819–828

Gong H, Blackmore D, Clingeleffer P, Sykes S, Jha D, Tester M, Walker R (2011) Contrast in chloride exclusion between two grapevine genotypes and its variation in their hybrid progeny. J Exp Bot **62:** 989–999

Guan R, Qu Y, Guo Y, Yu L, Liu Y, Jiang J, Chen J, Ren Y, Liu G, Tian L, et al (2014) Salinity tolerance in soybean is modulated by natural variation in GmSALT3. Plant J **80:** 937–950

Henderson SW, Baumann U, Blackmore DH, Walker AR, Walker RR, Gilliham M (2014) Shoot chloride exclusion and salt tolerance in grapevine is associated with differential ion transporter expression in roots. BMC Plant Biol **14:** 273

Henderson SW, Wege S, Qiu J, Blackmore DH, Walker AR, Tyerman SD, Walker RR, Gilliham M (2015) Grapevine and Arabidopsis cation-chloride cotransporters localise to the Golgi and trans-Golgi network and indirectly influence long-distance ion homeostasis and salt tolerance. Plant Physiol **169:** 2215–2229

Horie T, Hauser F, Schroeder JI (2009) HKT transporter-mediated salinity resistance mechanisms in Arabidopsis and monocot crop plants. Trends Plant Sci **14:** 660–668

James RA, Davenport RJ, Munns R (2006) Physiological characterization of two genes for Na^+ exclusion in durum wheat, *Nax1* and *Nax2*. Plant Physiol **142:** 1537–1547

Jeong J, Suh S, Guan C, Tsay Y-F, Moran N, Oh CJ, An CS, Demchenko KN, Pawlowski K, Lee Y (2004) A nodule-specific dicarboxylate transporter from alder is a member of the peptide transporter family. Plant Physiol **134:** 969–978

Jha D, Shirley N, Tester M, Roy SJ (2010) Variation in salinity tolerance and shoot sodium accumulation in *Arabidopsis* ecotypes linked to differences in the natural expression levels of transporters involved in sodium transport. Plant Cell Environ **33:** 793–804

Kamphake LJ, Hannah SA, Cohen JM (1967) Automated analysis for nitrate by hydrazine reduction. Water Res **1:** 205–216

Kanno Y, Hanada A, Chiba Y, Ichikawa T, Nakazawa M, Matsui M, Koshiba T, Kamiya Y, Seo M (2012) Identification of an abscisic acid transporter by functional screening using the receptor complex as a sensor. Proc Natl Acad Sci USA **109:** 9653–9658

Köhler B, Raschke K (2000) The delivery of salts to the xylem. Three types of anion conductance in the plasmalemma of the xylem parenchyma of roots of barley. Plant Physiol **122:** 243–254

Köhler B, Wegner LH, Osipov V, Raschke K (2002) Loading of nitrate into the xylem: apoplastic nitrate controls the voltage dependence of X-QUAC, the main anion conductance in xylem-parenchyma cells of barley roots. Plant J **30:** 133–142

Kollist H, Jossier M, Laanemets K, Thomine S (2011) Anion channels in plant cells. FEBS J **278:** 4277–4292

Kong X-Q, Gao X-H, Sun W, An J, Zhao Y-X, Zhang H (2011) Cloning and functional characterization of a cation-chloride cotransporter gene *OsCCC1*. Plant Mol Biol **75:** 567–578

Krouk G, Lacombe B, Bielach A, Perrine-Walker F, Malinska K, Mounier E, Hoyerova K, Tillard P, Leon S, Ljung K, et al (2010) Nitrate-regulated auxin transport by NRT1.1 defines a mechanism for nutrient sensing in plants. Dev Cell **18:** 927–937

Läuchli A, James RA, Huang CX, McCully M, Munns R (2008) Cell-specific localization of Na^+ in roots of durum wheat and possible control points for salt exclusion. Plant Cell Environ **31:** 1565–1574

Lee SC, Lan W, Buchanan BB, Luan S (2009) A protein kinase-phosphatase pair interacts with an ion channel to regulate ABA signaling in plant guard cells. Proc Natl Acad Sci USA **106:** 21419–21424

Léran S, Varala K, Boyer J-C, Chiurazzi M, Crawford N, Daniel-Vedele F, David L, Dickstein R, Fernandez E, Forde B, et al (2014) A unified nomenclature of NITRATE TRANSPORTER 1/PEPTIDE TRANSPORTER family members in plants. Trends Plant Sci **19:** 5–9

Li J-Y, Fu Y-L, Pike SM, Bao J, Tian W, Zhang Y, Chen C-Z, Zhang Y, Li H-M, Huang J, et al (2010) The *Arabidopsis* nitrate transporter NRT1.8 functions in nitrate removal from the xylem sap and mediates cadmium tolerance. Plant Cell **22:** 1633–1646

Lin SH, Kuo HF, Canivenc G, Lin CS, Lepetit M, Hsu PK, Tillard P, Lin HL, Wang YY, Tsai CB, Gojon A, Tsay YF (2008) Mutation of the *Arabidopsis* NRT1.5 nitrate transporter causes defective root-to-shoot nitrate transport. Plant Cell **20:** 2514–2528

Luo GZ, Wang HW, Huang J, Tian AG, Wang YJ, Zhang JS, Chen SY (2005) A putative plasma membrane cation/proton antiporter from soybean confers salt tolerance in *Arabidopsis*. Plant Mol Biol **59:** 809–820

Martin PK, Koebner RMD (1995) Sodium and chloride ions contribute synergistically to salt toxicity in wheat. Biol Plant **37:** 265–271

Mäser P, Hosoo Y, Goshima S, Horie T, Eckelman B, Yamada K, Yoshida K, Bakker EP, Shinmyo A, Oiki S, Schroeder JI, Uozumi N (2002) Glycine residues in potassium channel-like selectivity filters determine potassium selectivity in four-loop-per-subunit HKT transporters from plants. Proc Natl Acad Sci USA **99:** 6428–6433

Molendijk AJ, Ruperti B, Singh MK, Dovzhenko A, Ditengou FA, Milia M, Westphal L, Rosahl S, Soellick TR, Uhrig J, et al (2008) A cysteine-rich receptor-like kinase NCRK and a pathogen-induced protein kinase RBK1 are Rop GTPase interactors. Plant J **53:** 909–923

Møller IS, Gilliham M, Jha D, Mayo GM, Roy SJ, Coates JC, Haseloff J, Tester M (2009) Shoot Na^+ exclusion and increased salinity tolerance engineered by cell type-specific alteration of Na^+ transport in *Arabidopsis*. Plant Cell **21:** 2163–2178

Moya JL, Gómez-Cadenas A, Primo-Millo E, Talon M (2003) Chloride absorption in salt-sensitive *Carrizo citrange* and salt-tolerant *Cleopatra mandarin* citrus rootstocks is linked to water use. J Exp Bot **54:** 825–833

Munns R (2002) Comparative physiology of salt and water stress. Plant Cell Environ **25:** 239–250

Munns R, Gilliham M (2015) Salinity tolerance of crops - what is the cost? New Phytol **208:** 668–673

Munns R, James RA, Xu B, Athman A, Conn SJ, Jordans C, Byrt CS, Hare RA, Tyerman SD, Tester M, Plett D, Gilliham M (2012) Wheat grain yield on saline soils is improved by an ancestral Na^+ transporter gene. Nat Biotechnol **30:** 360–364

Munns R, Tester M (2008) Mechanisms of salinity tolerance. Annu Rev Plant Biol **59:** 651–681

Negi J, Matsuda O, Nagasawa T, Oba Y, Takahashi H, Kawai-Yamada M, Uchimiya H, Hashimoto M, Iba K (2008) CO_2 regulator SLAC1 and its homologues are essential for anion homeostasis in plant cells. Nature **452:** 483–486

Newstead S, Drew D, Cameron AD, Postis VLG, Xia X, Fowler PW, Ingram JC, Carpenter EP, Sansom MSP, McPherson MJ, Baldwin SA, Iwata S (2011) Crystal structure of a prokaryotic homologue of the mammalian oligopeptide-proton symporters, PepT1 and PepT2. EMBO J **30:** 417–426

Nour-Eldin HH, Andersen TG, Burow M, Madsen SR, Jørgensen ME, Olsen CE, Dreyer I, Hedrich R, Geiger D, Halkier BA (2012) NRT/PTR transporters are essential for translocation of glucosinolate defence compounds to seeds. Nature **488:** 531–534

Parker MB, Gascho GJ, Gaines TP (1983) Chloride toxicity of soybeans grown on atlantic coast flatwoods soils. Agron J **75:** 439–443

Peña L (2004) Transgenic Plants: Methods and Protocols. Humana Press, Totowa, New Jersey

Pitman M, Luttge U, Lauchli A, Ball E (1974) Effect of previous water stress on ion uptake and transport in barley seedlings. Funct Plant Biol **1:** 377–385

Pitman MG (1977) Ion transport into the xylem. Annu Rev Plant Physiol **28:** 71–88

Pitman MG (1982) Transport across plant roots. Q Rev Biophys **15:** 481–554

Plett D, Møller IS (2010) Na(+) transport in glycophytic plants: what we know and would like to know. Plant Cell Environ **33:** 612–626

Plett D, Safwat G, Gilliham M, Skrumsager Møller I, Roy S, Shirley N, Jacobs A, Johnson A, Tester M (2010) Improved salinity tolerance of rice through cell type-specific expression of *AtHKT1;1*. PLoS One **5:** e12571

Qiu L, Wu D, Ali S, Cai S, Dai F, Jin X, Wu F, Zhang G (2011) Evaluation of salinity tolerance and analysis of allelic function of *HvHKT1* and *HvHKT2* in Tibetan wild barley. Theor Appl Genet **122:** 695–703

Qiu Q-S, Guo Y, Dietrich MA, Schumaker KS, Zhu J-K (2002) Regulation of SOS1, a plasma membrane Na^+/H^+ exchanger in *Arabidopsis thaliana*, by SOS2 and SOS3. Proc Natl Acad Sci USA **99:** 8436–8441

Ren Z-H, Gao J-P, Li L-G, Cai X-L, Huang W, Chao D-Y, Zhu M-Z, Wang Z-Y, Luan S, Lin H-X (2005) A rice quantitative trait locus for salt tolerance encodes a sodium transporter. Nat Genet **37:** 1141–1146

Rengasamy P (2002) Transient salinity and subsoil constraints to dryland farming in Australian sodic soils: an overview. Aust J Exp Agric **42:** 351–361

Rengasamy P (2006) World salinization with emphasis on Australia. J Exp Bot **57:** 1017–1023

Roberts SK (1998) Regulation of K^+ channels in maize roots by water stress and abscisic acid. Plant Physiol **116:** 145–153

Roberts SK, Snowman BN (2000) The effects of ABA on channel-mediated $K(^+)$ transport across higher plant roots. J Exp Bot **51:** 1585–1594

Roy SJ, Gilliham M, Berger B, Essah PA, Cheffings C, Miller AJ, Davenport RJ, Liu LH, Skynner MJ, Davies JM, et al (2008) Investigating glutamate receptor-like gene co-expression in *Arabidopsis thaliana*. Plant Cell Environ **31:** 861–871

Roy SJ, Huang W, Wang XJ, Evrard A, Schmöckel SM, Zafar ZU, Tester M (2013) A novel protein kinase involved in Na^+ exclusion revealed from positional cloning. Plant Cell Environ **36:** 553–568

Roy SJ, Negrão S, Tester M (2014) Salt resistant crop plants. Curr Opin Biotechnol **26:** 115–124

Sali A, Blundell T (1994) Comparative protein modelling by satisfaction of spatial restraints. *In* H Bohr, S Brunak, eds, Protein Structure by Distance Analysis IOS Press, Amsterdam, pp 64–86

Sanders D (1980) The mechanism of Cl^- transport at the plasma membrane of *Chara corallina I*. Cotransport with H^+. J Membr Biol **53:** 129–141

Schwab R, Ossowski S, Riester M, Warthmann N, Weigel D (2006) Highly specific gene silencing by artificial microRNAs in Arabidopsis. Plant Cell **18:** 1121–1133

Segonzac C, Boyer JC, Ipotesi E, Szponarski W, Tillard P, Touraine B, Sommerer N, Rossignol M, Gibrat R (2007) Nitrate efflux at the root plasma membrane: identification of an *Arabidopsis* excretion transporter. Plant Cell **19:** 3760–3777

Shelden MC, Howitt SM, Kaiser BN, Tyerman SD (2009) Identification and functional characterisation of aquaporins in the grapevine, *Vitis vinifera*. Funct Plant Biol **36:** 1065–1078

Shen MY, Sali A (2006) Statistical potential for assessment and prediction of protein structures. Protein Sci **15:** 2507–2524

Shi H, Ishitani M, Kim C, Zhu JK (2000) The *Arabidopsis thaliana* salt tolerance gene SOS1 encodes a putative Na^+/H^+ antiporter. Proc Natl Acad Sci USA **97:** 6896–6901

Shi H, Quintero FJ, Pardo JM, Zhu J-K (2002) The putative plasma membrane Na^+/H^+ antiporter SOS1 controls long-distance Na^+ transport in plants. Plant Cell **14:** 465–477

Skerrett M, Tyerman SD (1994) A channel that allows inwardly directed fluxes of anions in protoplasts derived from wheat roots. Planta **192:** 295–305

Stacey G, Koh S, Granger C, Becker JM (2002) Peptide transport in plants. Trends Plant Sci **7:** 257–263

Storey R, Walker RR (1999) Citrus and salinity. Sci Hortic (Amsterdam) **78:** 39–81

Subramanian C, Woo J, Cai X, Xu X, Servick S, Johnson CH, Nebenführ A, von Arnim AG (2006) A suite of tools and application notes for in vivo protein interaction assays using bioluminescence resonance energy transfer (BRET). Plant J **48:** 138–152

Sun J, Bankston JR, Payandeh J, Hinds TR, Zagotta WN, Zheng N (2014) Crystal structure of the plant dual-affinity nitrate transporter NRT1.1. Nature **507:** 73–77

Sunarpi HT, Horie T, Motoda J, Kubo M, Yang H, Yoda K, Horie R, Chan WY, Leung HY, Hattori K, et al (2005) Enhanced salt tolerance mediated by AtHKT1 transporter-induced Na^+ unloading from xylem vessels to xylem parenchyma cells. Plant J **44:** 928–938

Nei M, Kumar S (2011) MEGA5: molecular evolutionary genetics analysis using maximum likelihood, evolutionary distance, and maximum parsimony methods. Mol Biol Evol **28:** 2731–2739

Taochy C, Gaillard I, Ipotesi E, Oomen R, Leonhardt N, Zimmermann S, Peltier JB, Szponarski W, Simonneau T, Sentenac H, Gibrat R, Boyer JC (2015) The *Arabidopsis* root stele transporter NPF2.3 contributes to nitrate translocation to shoots under salt stress. Plant J **83:** 466–479

Tavakkoli E, Fatehi F, Coventry S, Rengasamy P, McDonald GK (2011) Additive effects of Na^+ and Cl^- ions on barley growth under salinity stress. J Exp Bot **62:** 2189–2203

Teakle N, Flowers T, Real D, Colmer T (2007) *Lotus tenuis* tolerates the interactive effects of salinity and waterlogging by 'excluding' Na^+ and Cl^- from the xylem. J Exp Bot **58:** 2169–2180

Teakle NL, Tyerman SD (2010) Mechanisms of $Cl^{(-)}$ transport contributing to salt tolerance. Plant Cell Environ **33:** 566–589

Tester M, Davenport R (2003) Na^+ tolerance and Na^+ transport in higher plants. Ann Bot (Lond) **91:** 503–527

Tilman D, Balzer C, Hill J, Befort BL (2011) Global food demand and the sustainable intensification of agriculture. Proc Natl Acad Sci USA **108:** 20260–20264

Tregeagle JM, Tisdall JM, Blackmore DH, Walker RR (2006) A diminished capacity for chloride exclusion by grapevine rootstocks following long-term saline irrigation in an inland versus a coastal region of Australia. Aust J Grape Wine Res **12:** 178–191

Tsay YF, Chiu CC, Tsai CB, Ho CH, Hsu PK (2007) Nitrate transporters and peptide transporters. FEBS Lett **581:** 2290–2300

Tyerman SD (1992) Anion channels in plants. Annu Rev Plant Physiol Plant Mol Biol **43:** 351–373

Uozumi N, Kim EJ, Rubio F, Yamaguchi T, Muto S, Tsuboi A, Bakker EP, Nakamura T, Schroeder JI (2000) The Arabidopsis *HKT1* gene homolog mediates inward $Na(^+)$ currents in *xenopus laevis* oocytes and $Na(^+)$ uptake in *Saccharomyces cerevisiae*. Plant Physiol **122:** 1249–1259

Vahisalu T, Kollist H, Wang YF, Nishimura N, Chan WY, Valerio G, Lamminmäki A, Brosché M, Moldau H, Desikan R, Schroeder JI, Kangasjärvi J (2008) SLAC1 is required for plant guard cell S-type anion channel function in stomatal signalling. Nature **452:** 487–491

Vahisalu T, Puzõrjova I, Brosché M, Valk E, Lepiku M, Moldau H, Pechter P, Wang Y-S, Lindgren O, Salojärvi J, et al (2010) Ozone-triggered rapid stomatal response involves the production of reactive oxygen species, and is controlled by SLAC1 and OST1. Plant J **62:** 442–453

Waters S, Gilliham M, Hrmova M (2013) Plant High-Affinity Potassium (HKT) Transporters involved in salinity tolerance: structural insights to probe differences in ion selectivity. Int J Mol Sci **14:** 7660–7680

Weigel D, Glazebrook J (2002) Arabidopsis: A Laboratory Manual. Cold Spring Harbor Laboratory Press, Cold Spring Harbor, NY

White PJ, Broadley MR (2001) Chloride in soils and its uptake and movement within the plant: A review. Ann Bot (Lond) **88:** 967–988

Wu S, Zhang Y (2007) LOMETS: a local meta-threading-server for protein structure prediction. Nucleic Acids Res **35:** 3375–3382

Wu SJ, Ding L, Zhu JK (1996) *SOS1*, a genetic locus essential for salt tolerance and potassium acquisition. Plant Cell **8:** 617–627

Xu G, Magen H, Tarchitzky J, Kafkafi U (1999) Advances in chloride nutrition of plants. *In* LS Donald, ed, Advances in Agronomy, **Vol 68**. Academic Press, Cambridge, pp 97–150

Yamashita T, Shimada S, Guo W, Sato K, Kohmura E, Hayakawa T, Takagi T, Tohyama M (1997) Cloning and functional expression of a brain peptide/histidine transporter. J Biol Chem **272:** 10205–10211

Yoo S-D, Cho Y-H, Sheen J (2007) Arabidopsis mesophyll protoplasts: a versatile cell system for transient gene expression analysis. Nat Protoc **2:** 1565–1572

Zhou J-J, Theodoulou FL, Muldin I, Ingemarsson B, Miller AJ (1998) Cloning and functional characterization of a *Brassica napus* transporter that is able to transport nitrate and histidine. J Biol Chem **273:** 12017–12023